Supplementary Fig. 1

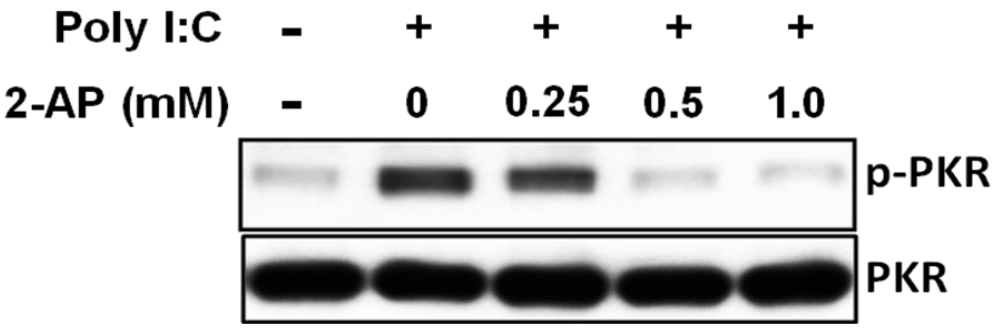

Supplementary Fig 1. PKR inhibitor 2-AP dose-dependently inhibited Poly I:C-induced PKR phosphorylation. PMA-differentiated THP-1 human macrophages were transfected with Poly I:C/Lyovec^{TM} for 4 h in the presence of indicated concentration of 2-AP. PKR phosphorylation and total PKR level in cell lysates were assessed by western-blot. Results are representative of 2 independent experiments.

Supplementary Fig. 2

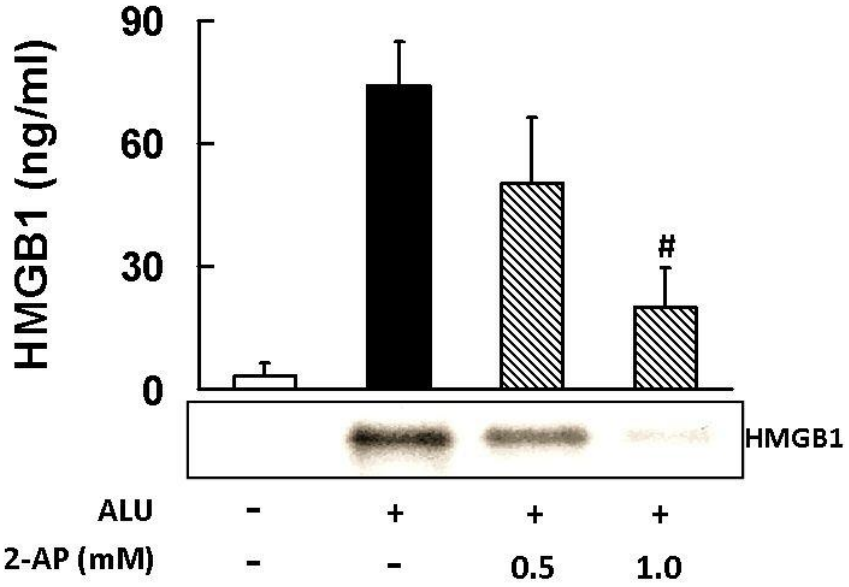

Supplementary Fig. 2. PKR inhibitor 2-AP significantly inhibited ALU-induced HMGB1 release. Ultra-pure LPS-primed mouse $PKR^{+/+}$ macrophages were stimulated with ALU for 6h in the absence or the presence of 2-AP at the indicated concentration. HMGB1 level in supernatant was assessed by Western-blot. #, $p<0.05$ vs. stimulated groups in the absence of 2-AP.

Supplementary Fig. 3

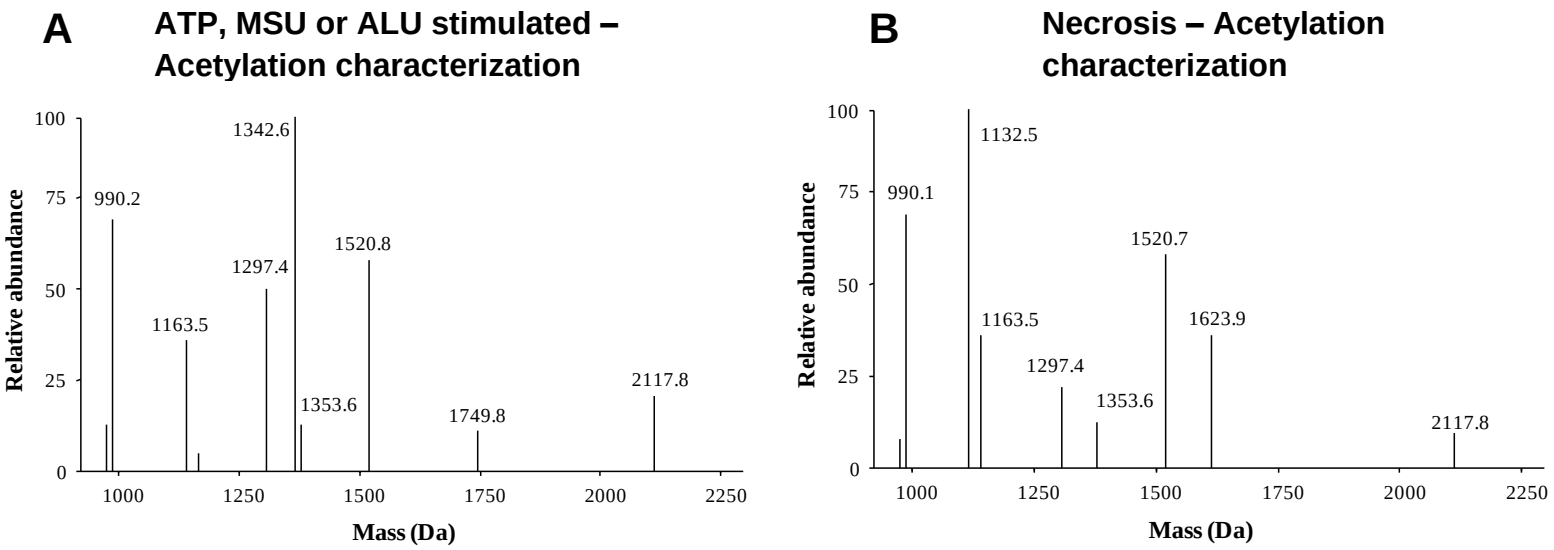

Supplementary Fig. 3. Mass spectrometric characterization of acetyl post-translational modifications of trypic and Glu-C derived peptides of HMGB1 released by macrophage in response to ATP, MSU or ALU (A) or HMGB1 released from macrophages subjected to freeze/thaw cycles (B).

Supplementary Fig. 4

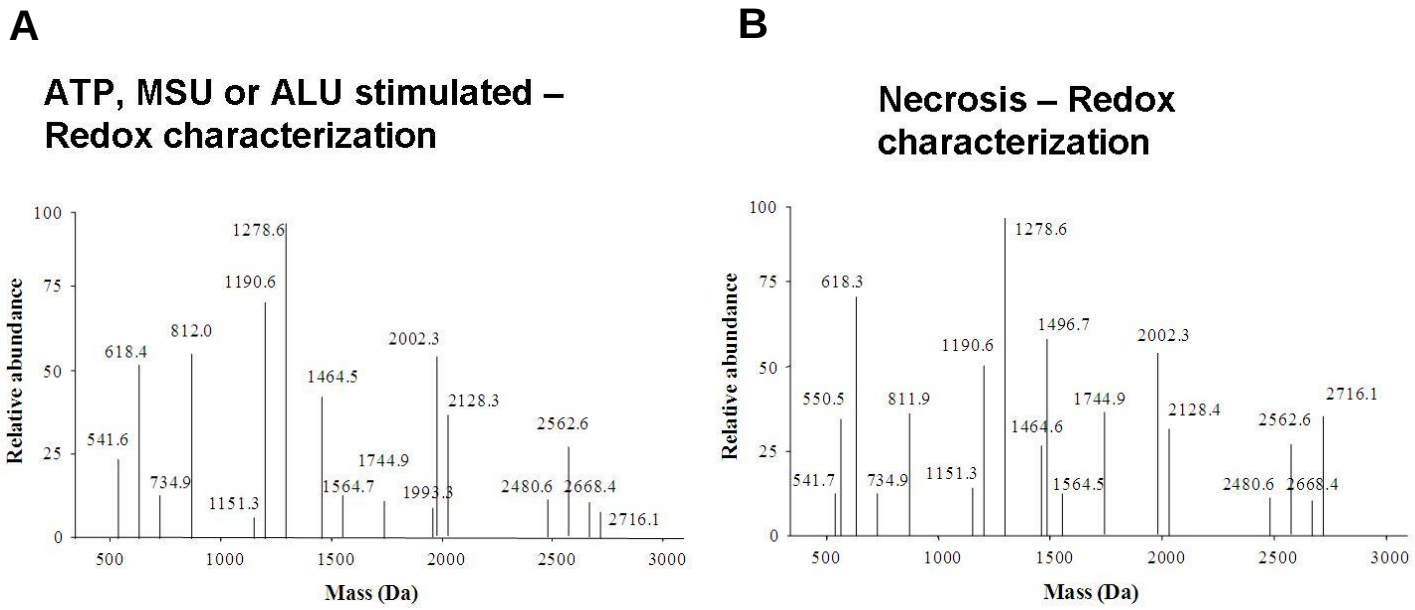

Supplementary Fig. 4. Mass spectrometric characterization of redox status of trypic and Glu-C derived peptides of HMGB1 released by macrophage in response to ATP, MSU or ALU (A) or HMGB1 released from macrophages subjected to freeze/thaw cycles (B). Mass-spectrometric analysis of redox status of 3 cysteines (C23, C45, and C106) of HMGB1 (C).

Supplementary Fig. 5

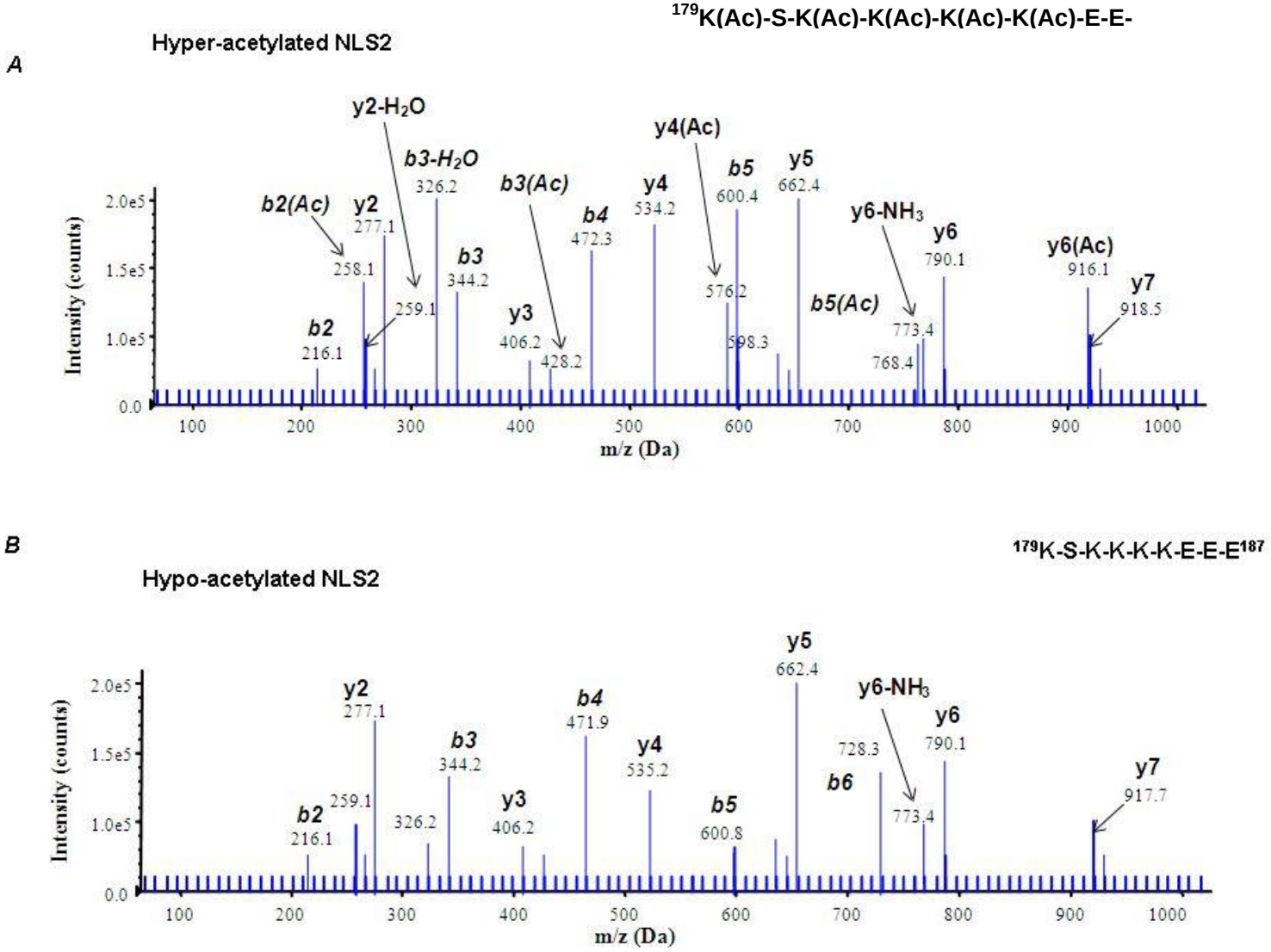

Supplementary Fig. 5. Representative MS/MS spectra of HMGB1 amino acids 179-187 derived from the HMGB1 NLS2 containing acetylated (A) or non-acetylated (B) lysine residues.

Supplementary Fig. 6

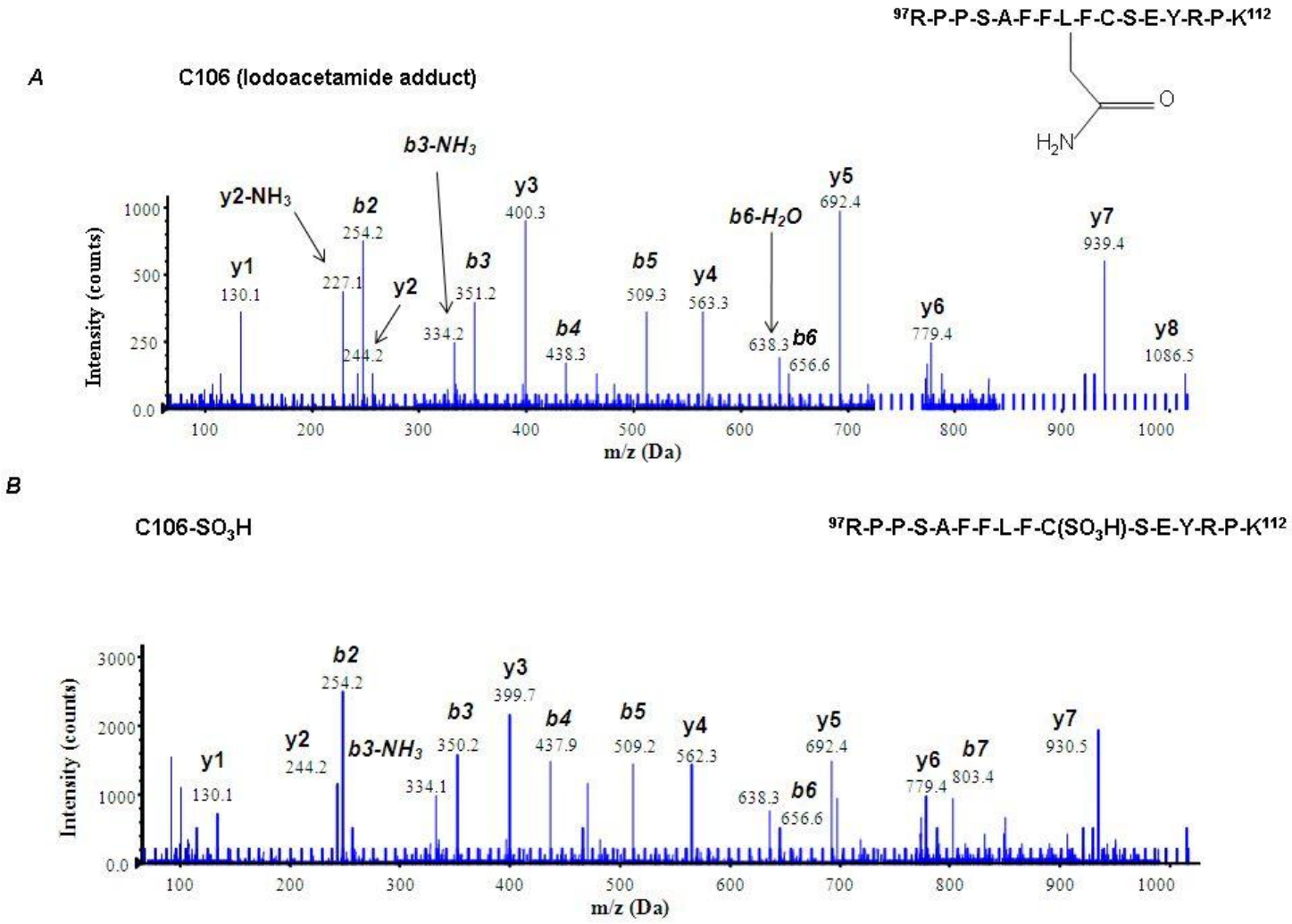

Supplementary Fig. 6. Representative MS/MS spectra of HMGB1 amino acids 97-112 with either an iodoacetamide capped (A) or terminally oxidized (B) cysteine residue following trypsin digestion.

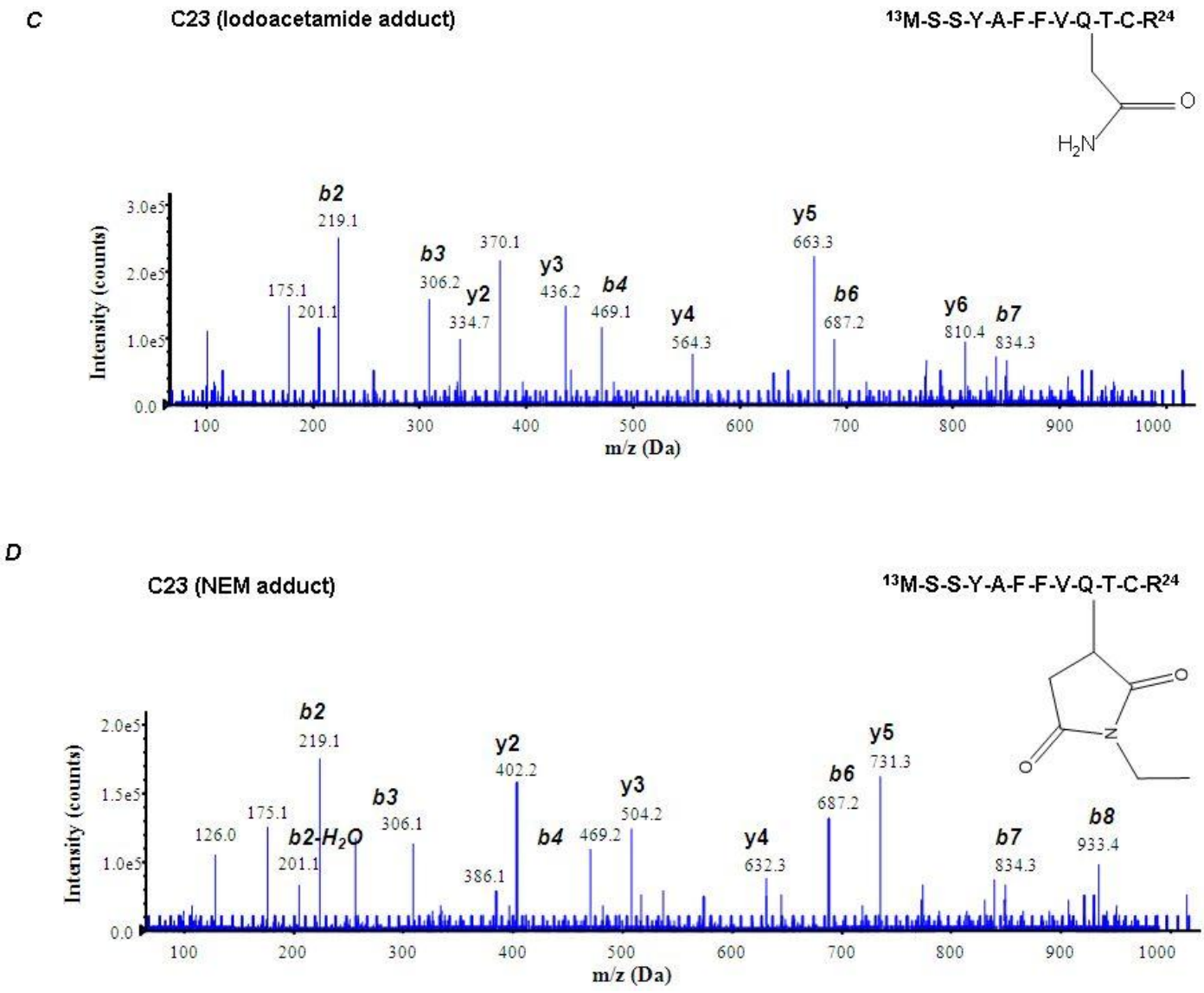

Representative MS/MS spectra of HMGB1 amino acids 13-24 from an iodoacetamide (C) or NEM (D) capped cysteine residue following trypsin digestion.

E

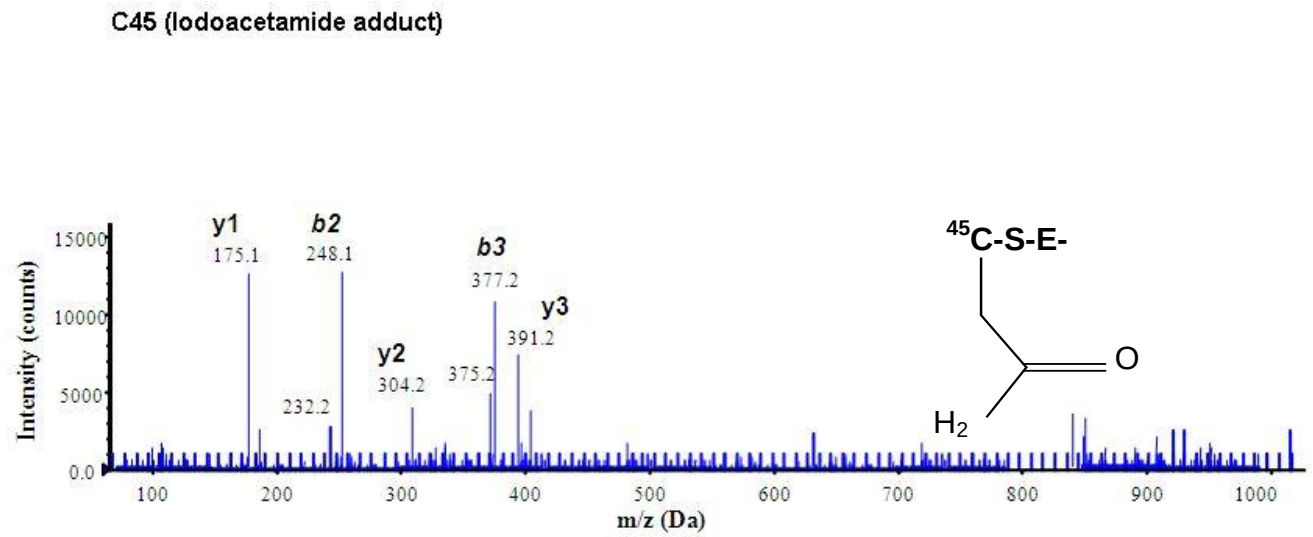

F

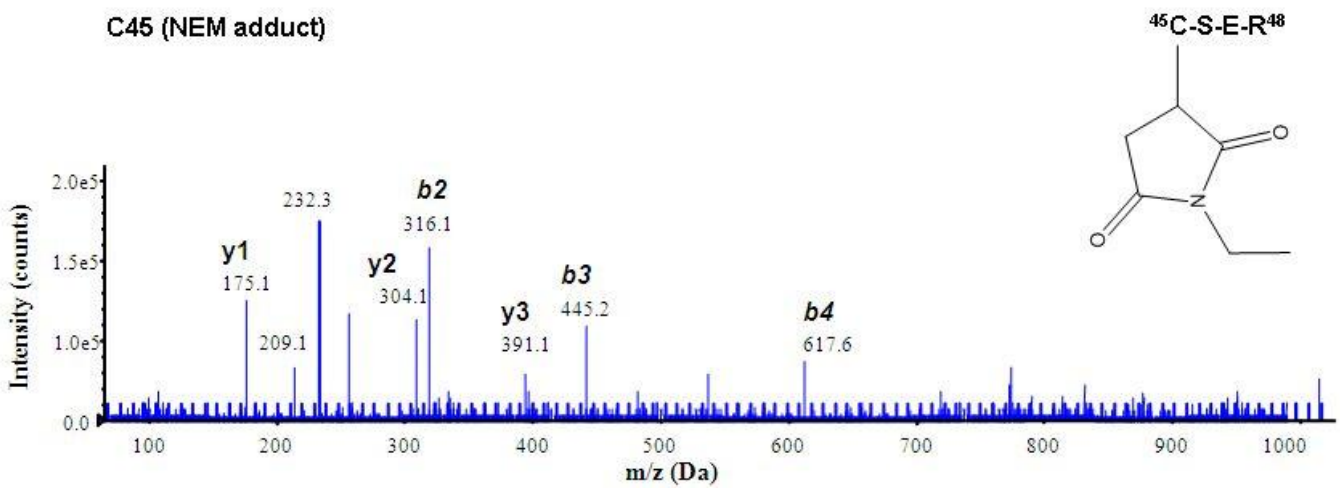

Representative MS/MS spectra of HMGB1 amino acids 45-48 from an iodoacetamide (E) or NEM (F) capped cysteine residue following trypsin digestion.

Supplementary Fig. 7

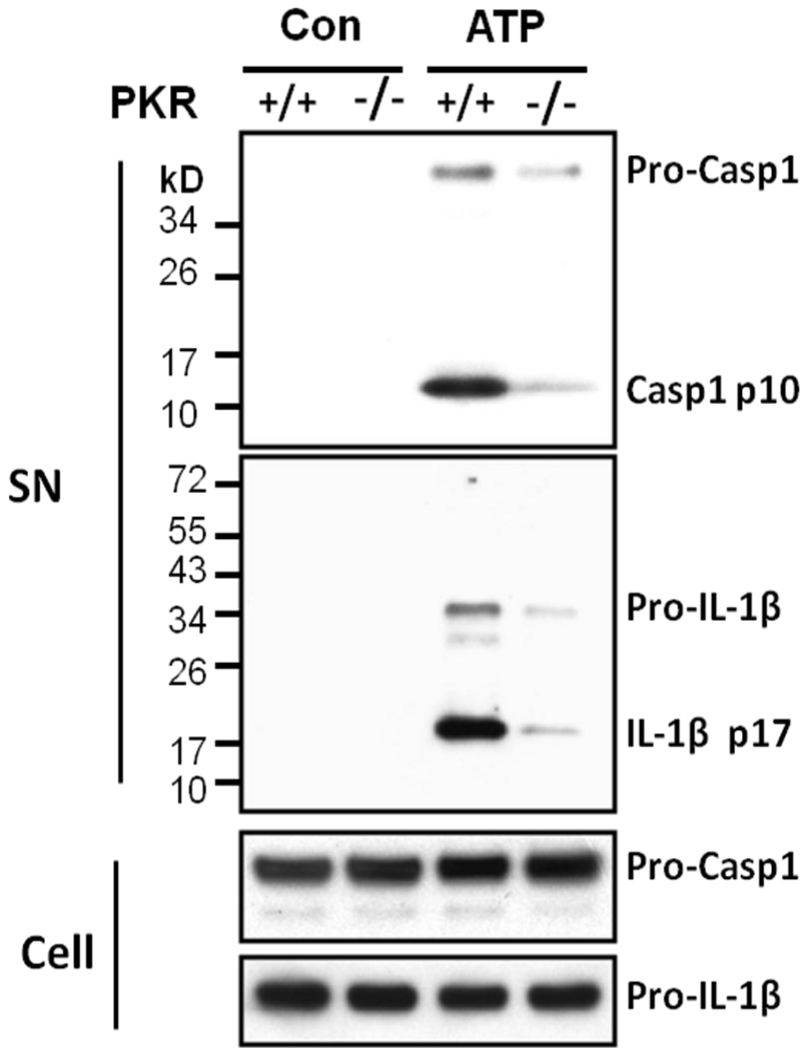

Supplementary Fig. 7. PKR is important for ATP-induced inflammasome activation in bone-marrow-derived dendritic cells. Ultra-pure LPS-primed mouse bone-marrow-derived-dendritic cells from $PKR^{+/+}$ or $PKR^{-/-}$ mice were stimulated with ATP (5 mM) for 40 min. Caspase-1 activation and IL-1β maturation was assessed by Western-blot. Results are representative of 3 independent experiments.

Supplementary Fig. 8

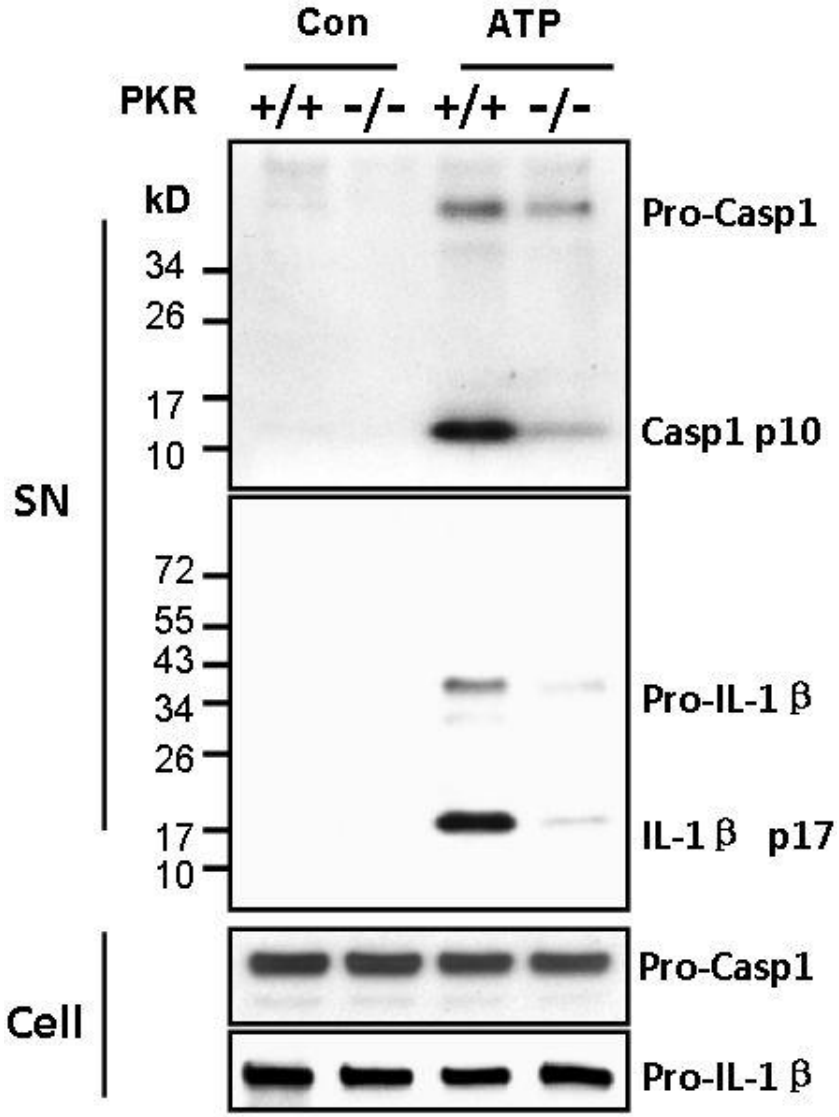

Supplementary Fig. 8. PKR is important for ATP-induced inflammasome activation in bone-marrow-derived-macrophages. Ultra-pure LPS-primed bone-marrow-derived-macrophages from $PKR^{+/+}$ or $PKR^{-/-}$ mice were stimulated with ATP (5 mM) for 40 min. Caspase-1 activation and IL-1β maturation was assessed by Western-blot. Results are representative of 3 independent experiments.

Supplementary Fig. 9

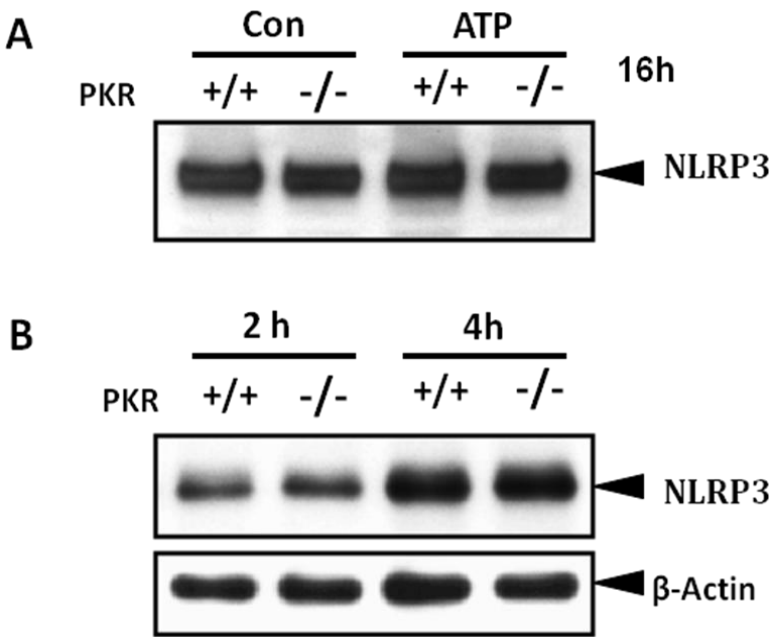

Supplementary Fig. 9. PKR has no effect on the expression of NLRP3 in macrophages and dendritic cells. Dendritic cells (A) or peritoneal macrophages (B) from $PKR^{+/+}$ or $PKR^{-/-}$ mice were primed with Ultra-pure LPS for indicated time (2h, 4h, or 16h), with or without stimulation of ATP (5 mM) for 30 min. Cell lysis was obtained and the NLRP3 expression was assessed by Western-blot. Results are representative of 3 independent experiments.

Supplementary Fig. 10

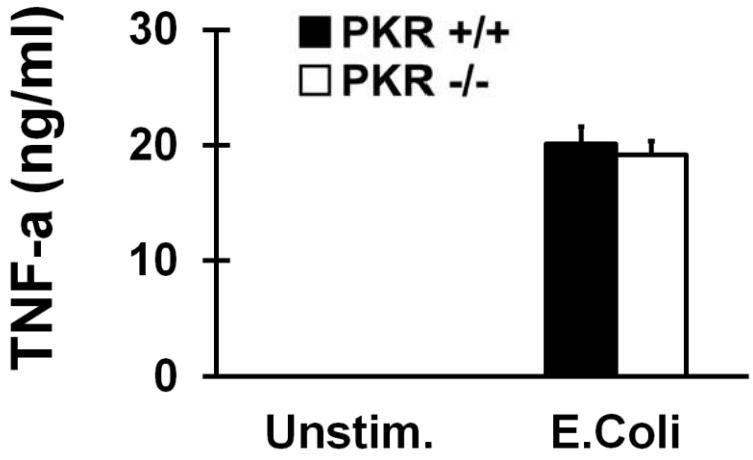

Supplementary Fig. 10. PKR deficiency did not alter TNF production *in vivo*. $PKR^{+/+}$ or $PKR^{-/-}$ mouse macrophages were infected live *E. coli* (MOI=20) for 6 h, Levels of TNF in the supernatant were determined by ELISA.

Supplementary Fig 11

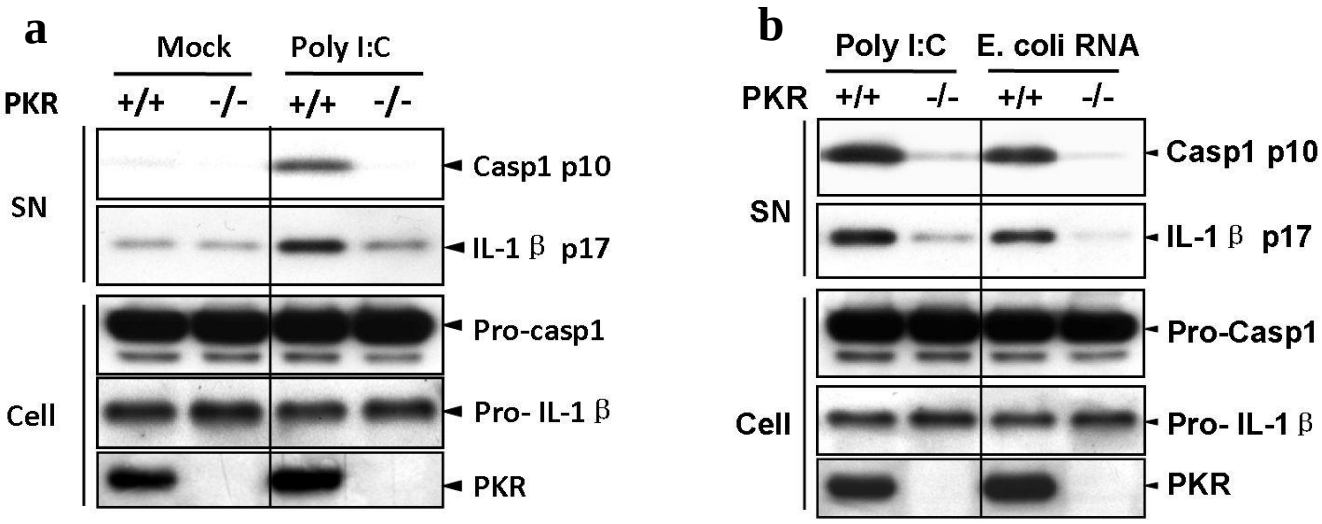

Supplementary Fig. 11. PKR regulates Poly I:C or *E.coli* RNA transfection-induced inflammasome activation. a. Ultra-pure LPS-primed bone-marrow-derived-dendritic cells from $PKR^{+/+}$ or $PKR^{-/-}$ mice were transfected with Poly I:C by lipofectamine for 6h. b. Ultra-pure LPS-primed bone-marrow-derived-dendritic cells from $PKR^{+/+}$ or $PKR^{-/-}$ mice were transfected with Poly I:C or *E. coli* RNA by electroporation for 4h. Caspase-1 activation and IL-1β maturation was assessed by Western-blot. Results are representative of 3 independent experiments.

Supplementary Fig. 12

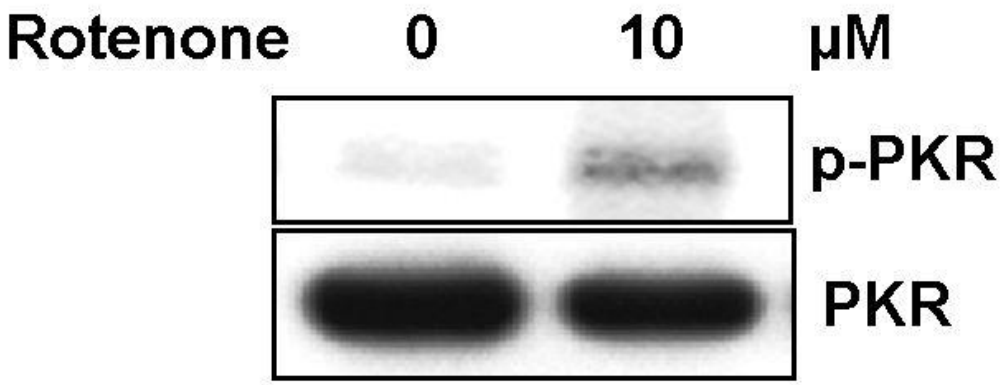

Supplementary Fig. 12. Rotenone induces PKR phosphorylation. LPS-primed $PKR^{+/+}$ macrophages were stimulated with rotenone (10 μM). Cells were lysed 2h after stimulation and PKR activation was monitored by autophosphorylation. Results are representative of 3 independent experiments.

Supplementary Fig. 13

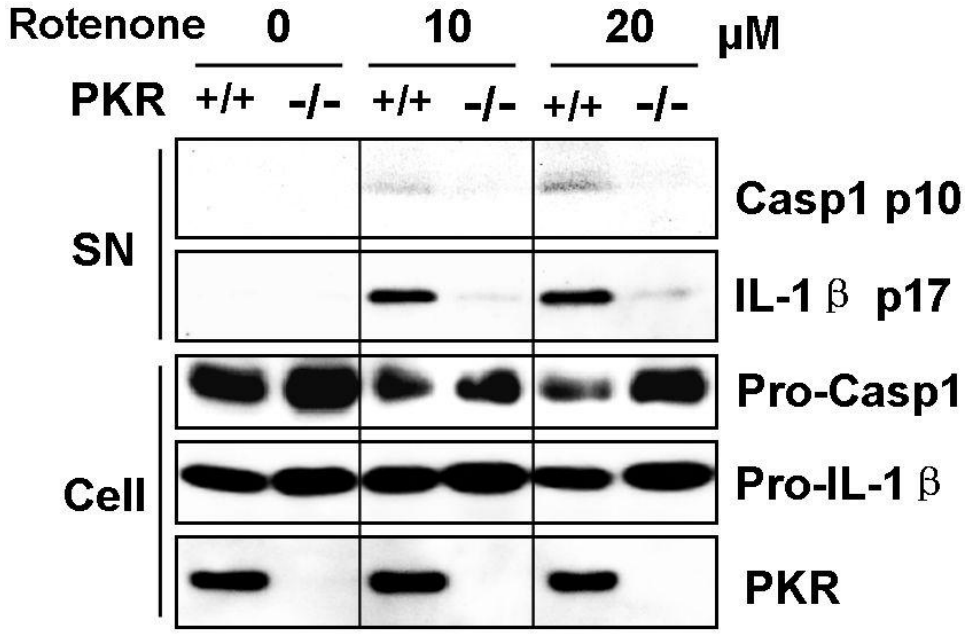

Supplementary Fig. 13. PKR is important for rotenone-induced inflammasome activation. Ultra-pure LPS-primed peritoneal $PKR^{+/+}$ or $PKR^{-/-}$ macrophages were stimulated with rotenone for 6 h. Caspase-1 activation and IL-1β maturation was assessed by Western-blot. Results are representative of 3 independent experiments.

Supplementary Fig. 14

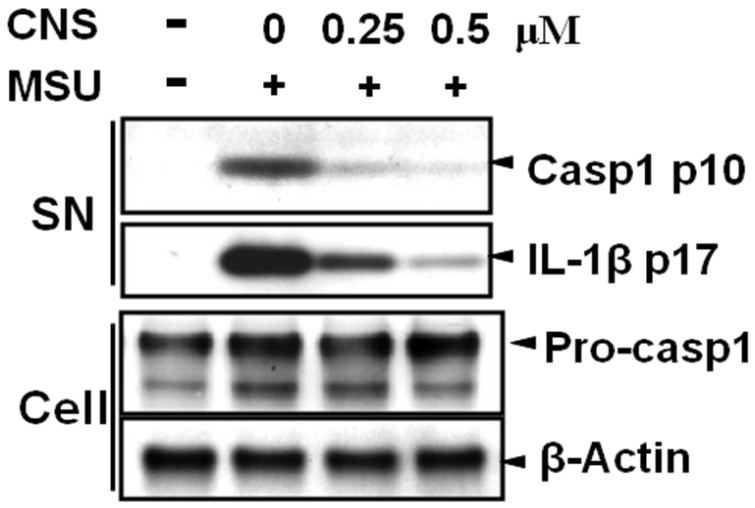

Supplementary Fig. 14. PKR inhibitor CNS dose-dependently inhibits MSU-induced inflammasome activation. Ultra-pure LPS-primed mouse $PKR^{+/+}$ macrophages were stimulated with MSU (150 μg/ml) for 6 h in the presence of $C_{13}H_8N_4OS$ (CNS) at the indicated concentration. Caspase-1 activation and IL-1β maturation was assessed by Western-blot. Results are representative of 3 independent experiments.

Supplementary Fig. 15

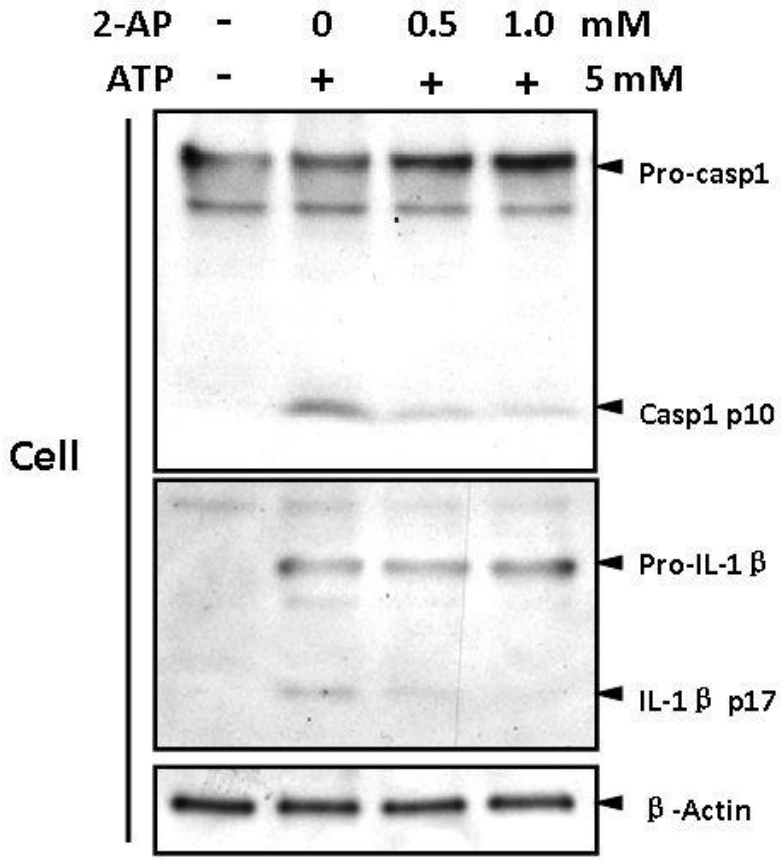

Supplementary Fig. 15. PKR inhibitor 2-AP dose-dependently inhibits ATP-induced inflammasome activation. Ultra-pure LPS-primed mouse macrophages from wild-type mice were stimulated with ATP (5 mM) for 30 min in the absence or the presence of 2-AP at the indicated concentration. Cell lysis was obtained, and caspase-1 activation and IL-1β maturation were assessed by Western-blot. Results are representative of 2 independent experiments.

Supplementary Fig. 16

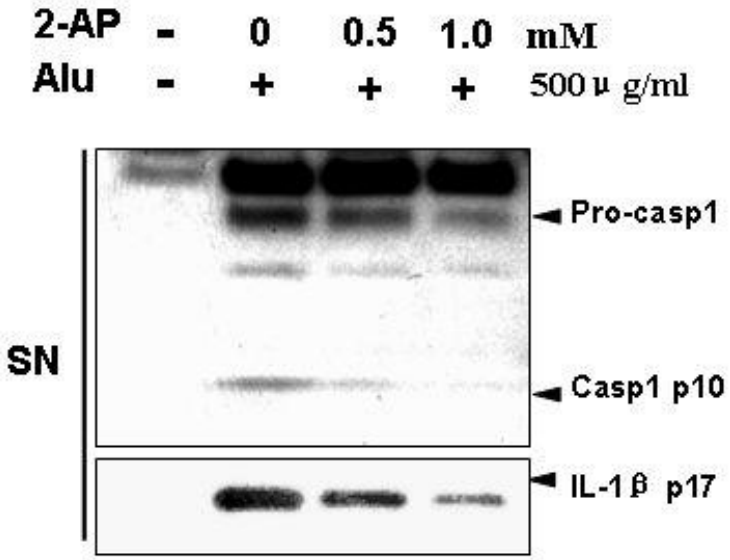

Supplementary Fig. 16. PKR inhibitor 2-AP dose-dependently inhibits ALU-induced inflammasome activation. Ultra-pure LPS-primed mouse macrophages from wild-type mice were stimulated with ALU (200 μg/ml) for 5 h in the absence or the presence of 2-AP at the indicated concentration. Caspase-1 activation and IL-1β maturation were assessed by Western-blot. Results are representative of 3 independent experiments.

Supplementary Figure 17

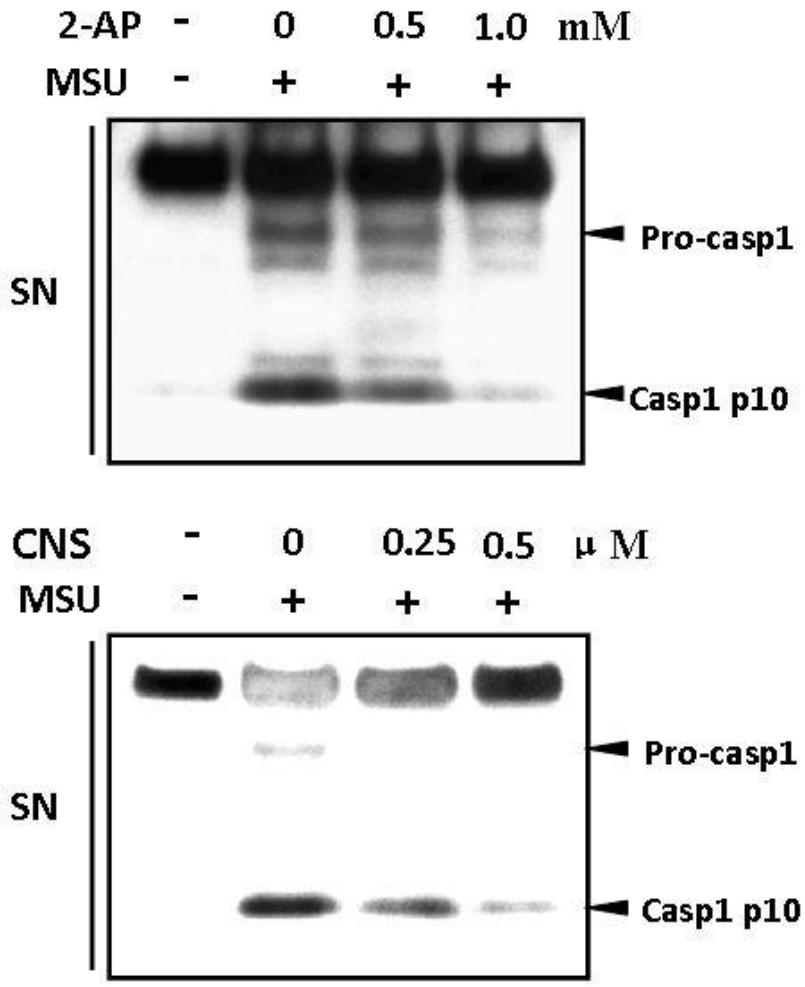

Supplementary Fig. 17. PKR inhibitor 2-AP dose-dependently inhibits MSU-induced inflammasome activation in human THP-1 cells. PMA-differentiated THP-1 human macrophages were stimulated with MSU (150 µg/ml) in the absence or the presence of 2-AP or $C_{13}H_8N_4OS$ at the indicated concentration. Caspase-1 activation was assessed by Western-blot. Results are representative of 2 independent experiments.

Supplementary Fig. 18

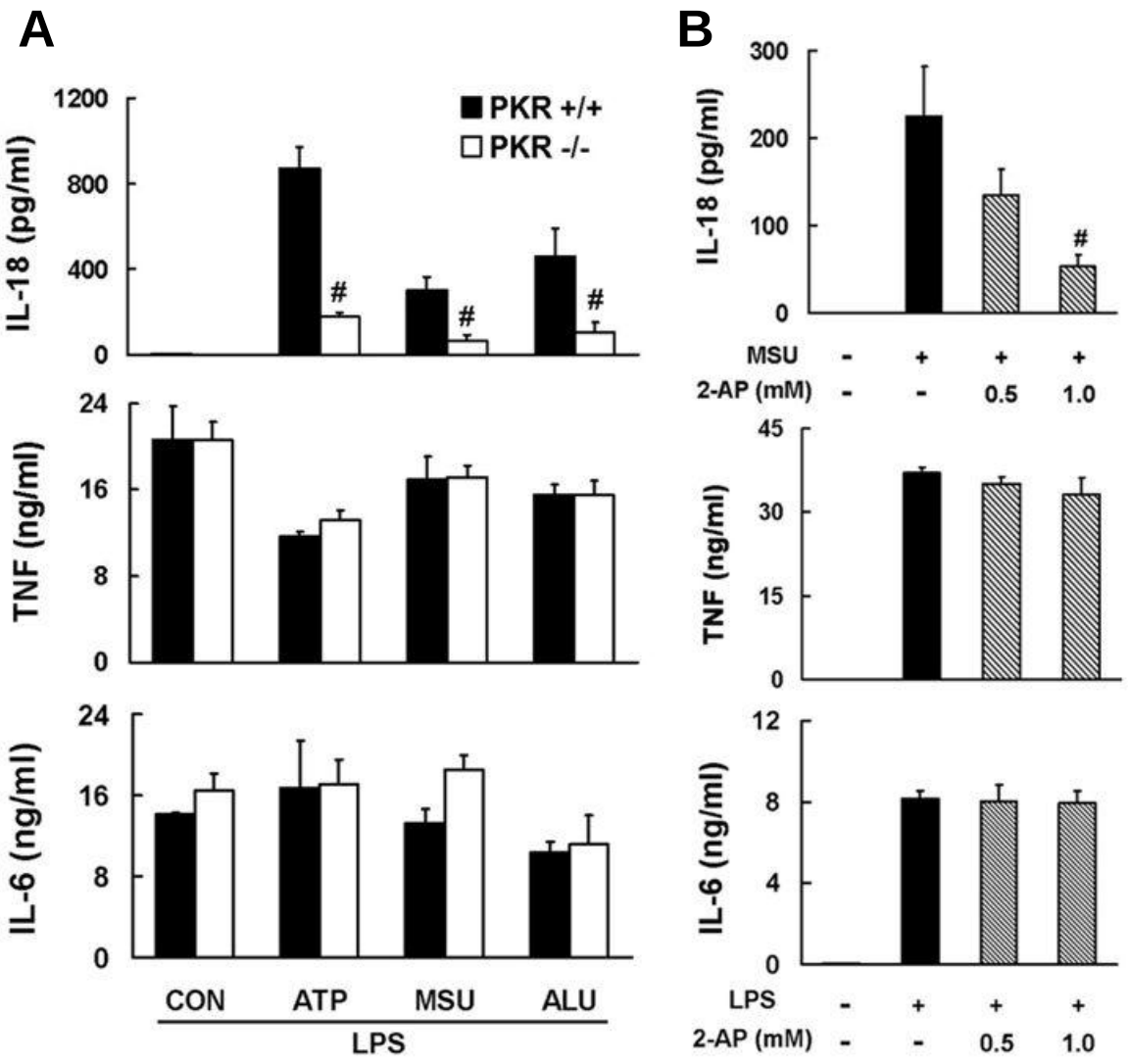

Supplementary Fig. 18. PKR regulates the release of inflammasome-dependent cytokines *in vitro*. A. Ultra-pure LPS-primed $PKR^{+/+}$ or $PKR^{-/-}$ macrophages were stimulated with ATP, MSU, or ALU. **B.** $PKR^{+/+}$ macrophages were stimulated and treated with 2-AP as indicated. IL-18, TNF, and IL-6 levels were measured in the supernatant by ELISA. Data shown are means ± SD. #, $p<0.05$ vs. wild-type stimulated groups.

Supplementary Fig. 19

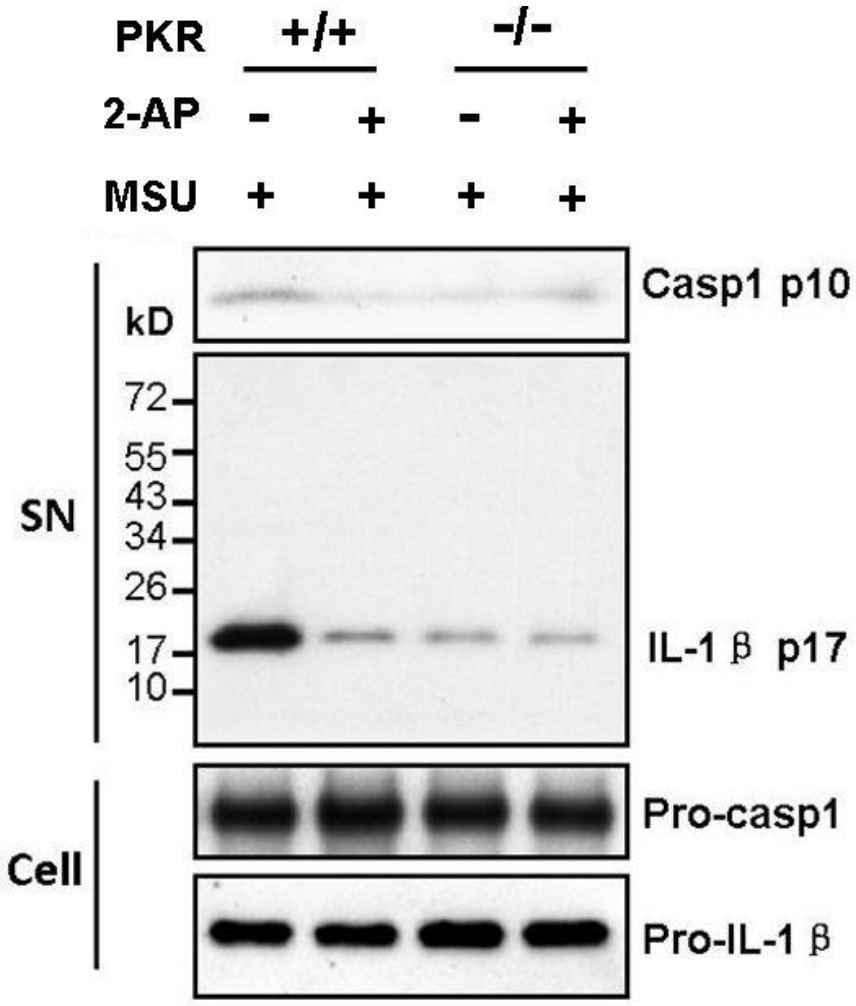

Supplementary Fig. 19. PKR inhibitor 2-AP did not further inhibit caspases-1 activation and IL-1β cleavage in PKR$^{-/-}$ macrophages. Ultra-pure LPS-primed PKR$^{+/+}$ or PKR$^{-/-}$ peritoneal macrophages were stimulated with MSU (150 μg/ml) in the presence or the absence of 2-AP (1 mM). Caspase-1 activation and IL-1β maturation were assessed by Western-blot. Results are representative of 3 independent experiments.

Supplementary Fig. 20

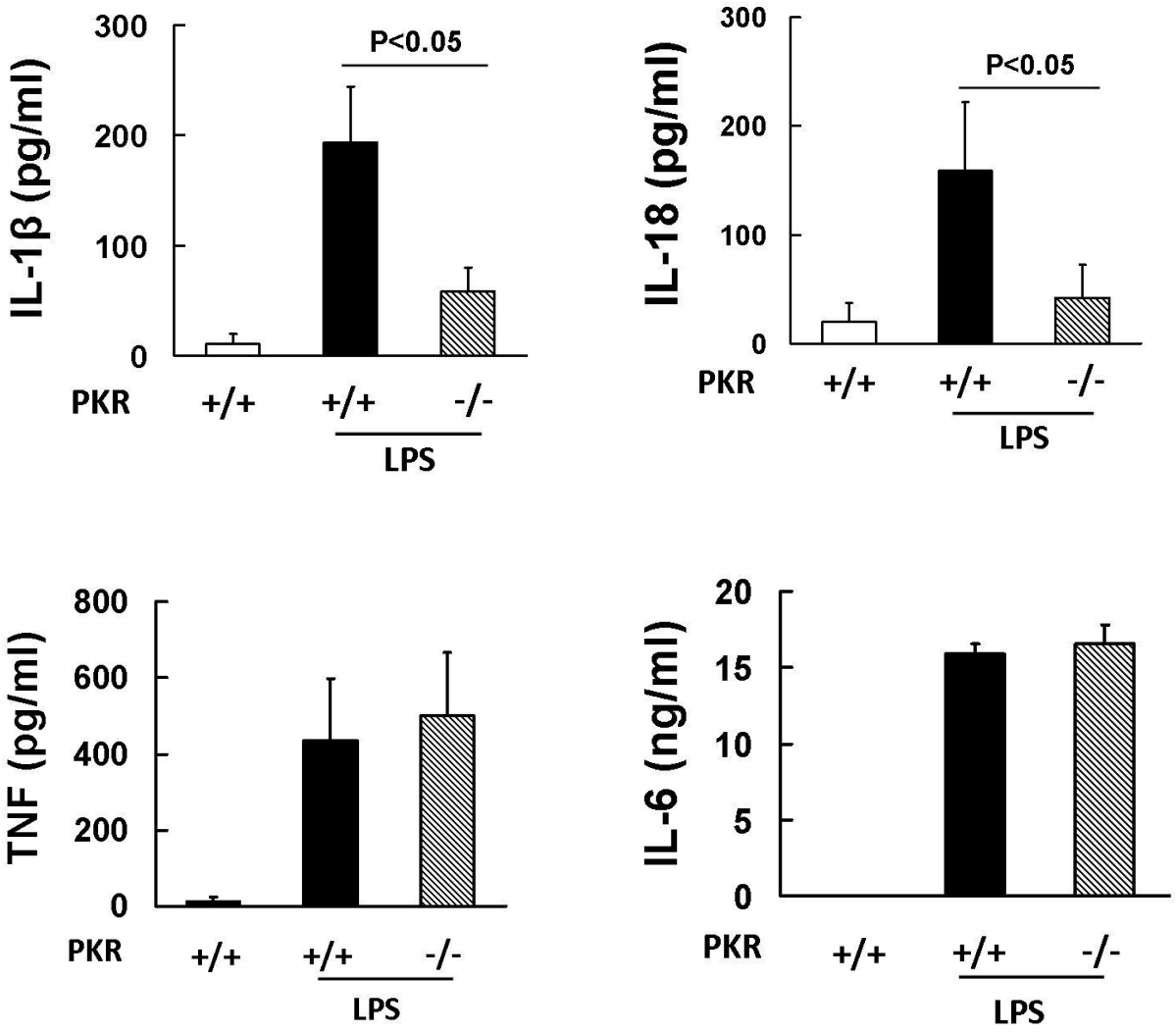

Supplementary Fig. 20. PKR regulates inflammasome-dependent cytokine release during endotoxemia. $PKR^{+/+}$ or $PKR^{-/-}$ mice (n=5) were injected with LPS. Serum levels of IL-1β, IL-18, TNF, and IL-6 were measured by ELISA. Data shown are means ± SD.

Supplementary Fig. 21

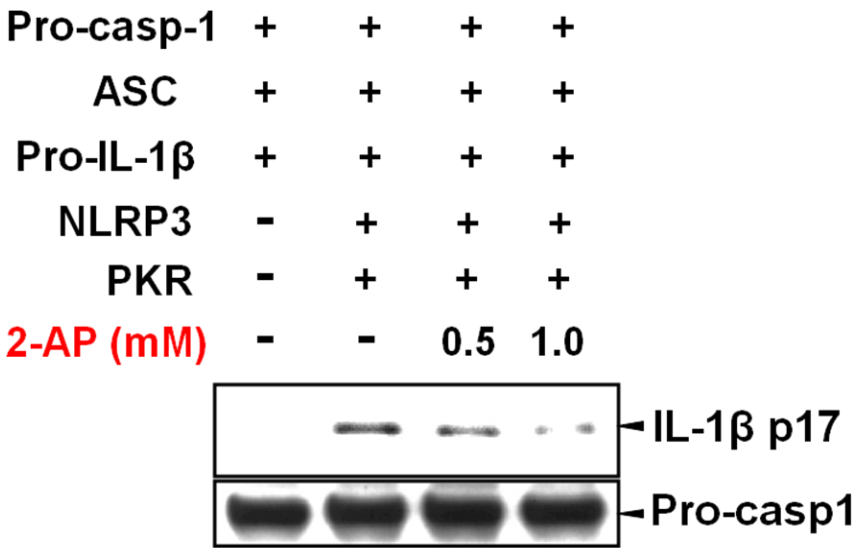

Supplementary Fig. 21. PKR inhibitor 2-AP dose-dependently inhibits the reconstituted inflammasome-mediated IL-1β cleavage. HEK293A cells were transfected as indicated for 24 h. IL-1β cleavage was assessed by Western-blot. Results are representative of 2 independent experiments.

Supplementary Fig. 22

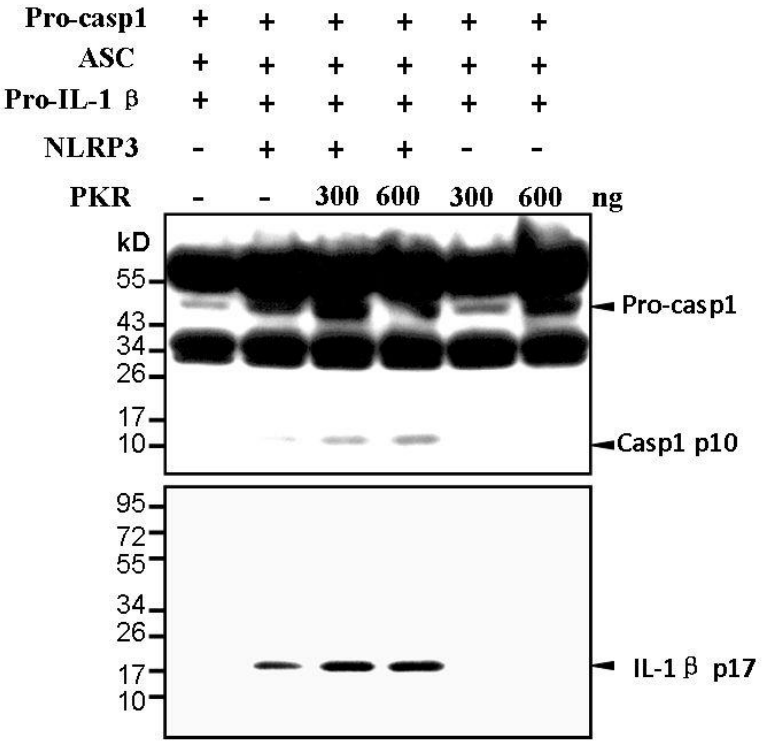

Supplementary Fig. 22. PKR overexpression failed to directly activate caspase-1 and IL-1β maturation in the absence of NLRP3. HEK293A cells were transfected as indicated for 24 h. Caspase-1 activation and IL-1β maturation was assessed by Western-blot. Results are representative of 2 independent experiments.

Supplementary Fig. 23

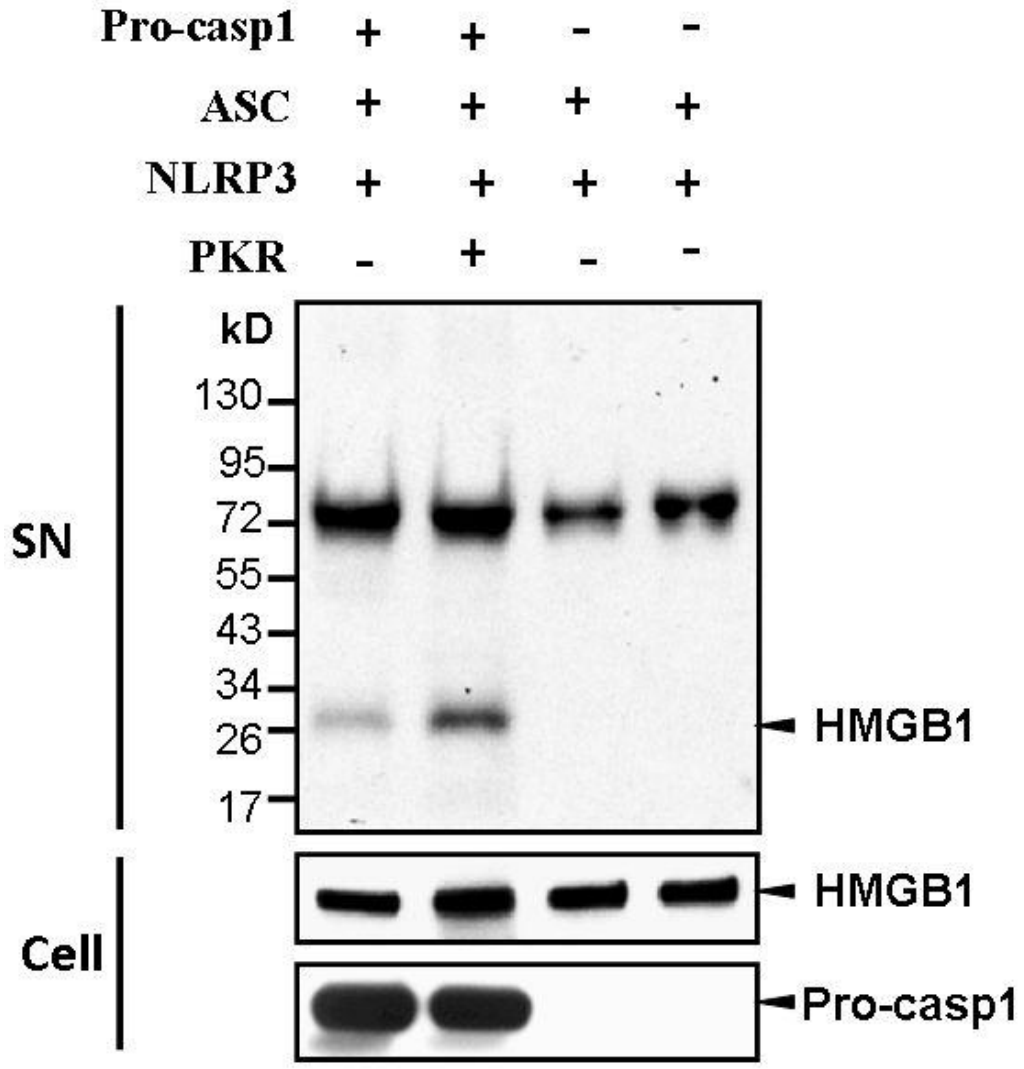

Supplementary Fig. 23. PKR overexpression increases HMGB1 release via a caspases-1 dependent mechanism. HEK293A cells were transfected as indicated for 20 h. HMGB1 in cell culture medium and cell lysates were assessed by Western-blot. Results are representative of 2 independent experiments.

Supplementary Fig. 24

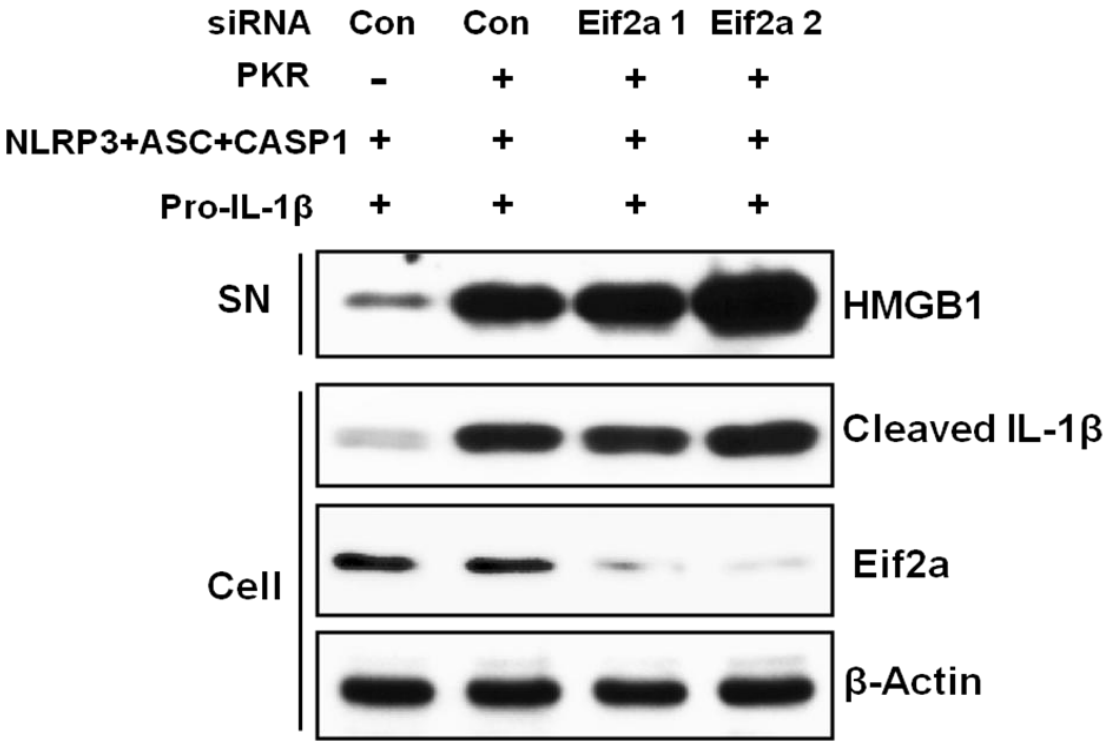

Supplementary Fig. 24. Knock-down of endogenous eIF-2a did not alter HMGB1 release and IL-1β cleavage in the NLRP3 inflammasome-reconstituted cells. HEK293A cells were transfected as indicated (siRNA were transfected 24h before the transfection of DNA plasmids). HMGB1 secretion and IL-1β cleavage were assessed by Western-blot. Results are representative of 2 independent experiments.

Supplementary Fig. 25

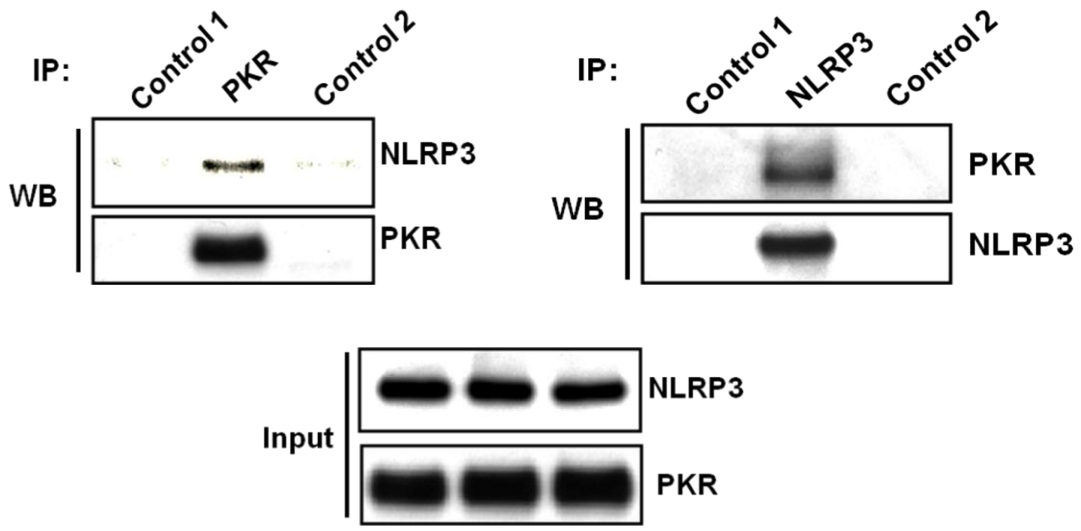

Supplementary Fig. 25. PKR physically interacts with NLRP3 in mouse macrophages. Immunoprecipitation (IP) and Western-blot (WB) analysis of the physical interaction of PKR and NLRP3 in LPS-primed $PKR^{+/+}$ macrophages. Results are representative of three independent experiments.

Supplementary Fig. 26

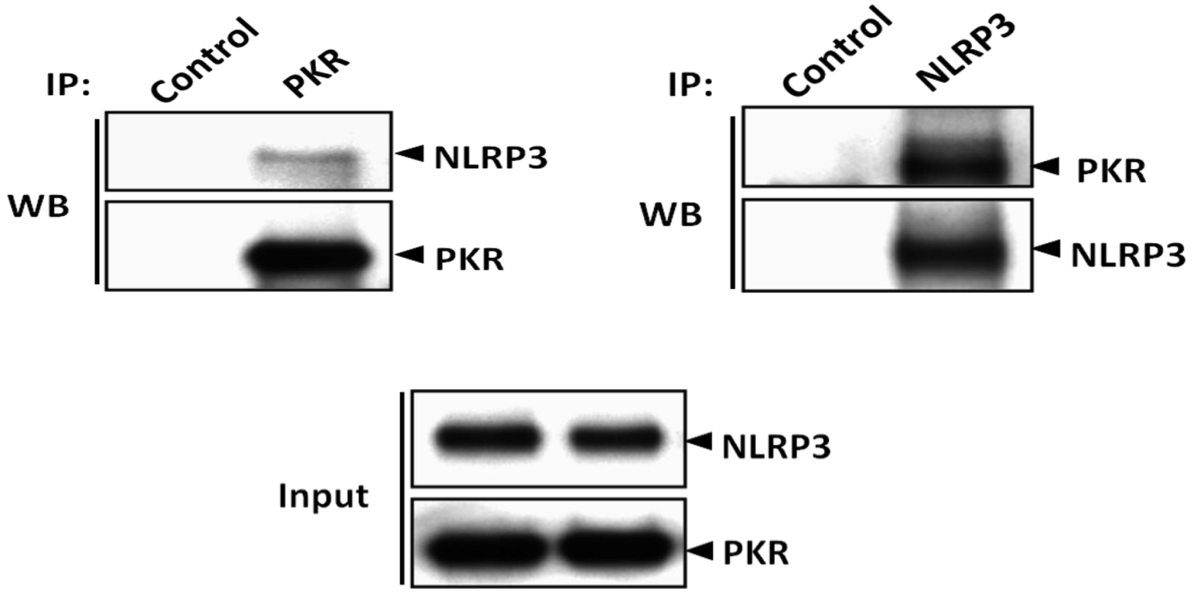

Supplementary Fig. 26. PKR physically interacts with the NLRP3 in human THP-1 cells. Immunoprecipitation (IP) and Western-blot (WB) analysis of the physical interaction of PKR and NLRP3 in PMA-differentiated THP-1 human macrophages. Results are representative of 2 independent experiments.

Supplementary Fig. 27

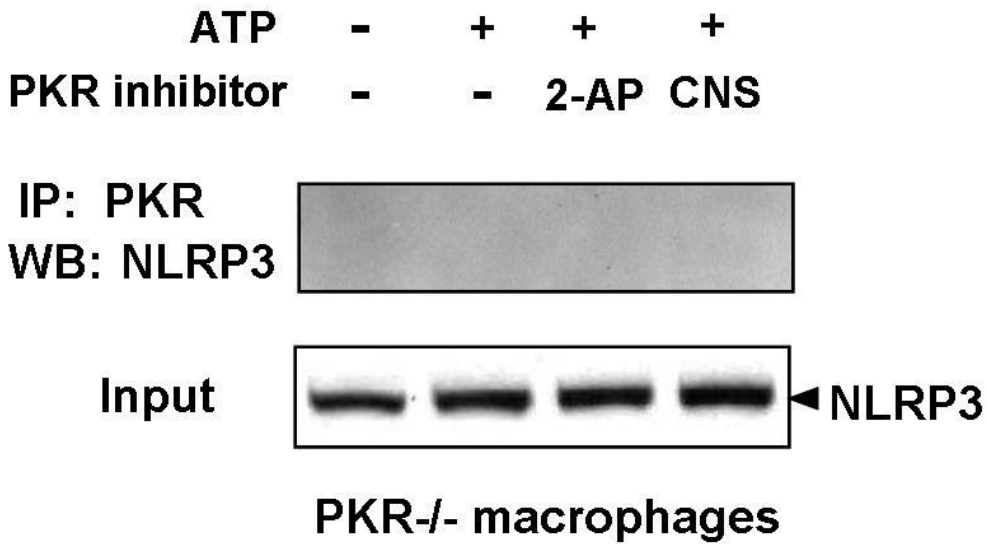

Supplementary Fig. 27. PKR-NLRP3 complexes could not be detected in the PKR$^{-/-}$ macrophages. Immunoprecipitation (IP) and Western-blot (WB) analysis of the physical interaction of PKR and NLRP3 in PKR$^{-/-}$ macrophages. Results are representative of 2 independent experiments.

Supplementary Fig. 28.

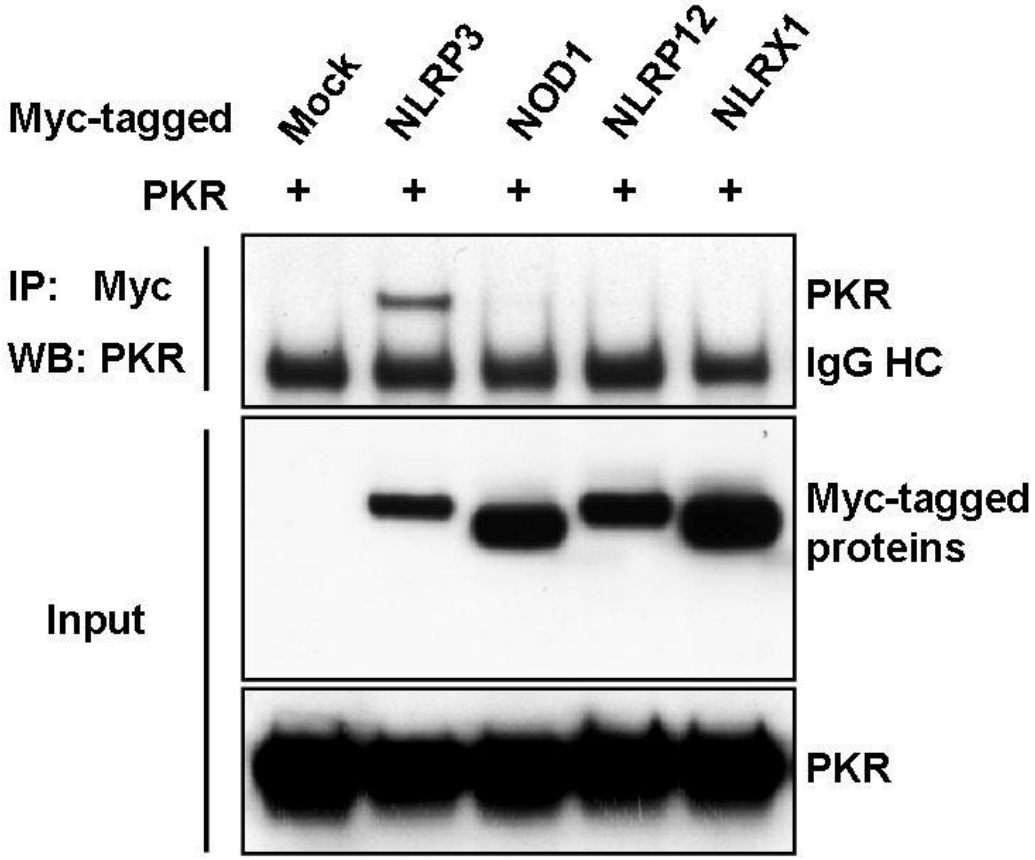

Supplementary Fig. 28. PKR physically interact with NLRP3. Myc-tagged NLRP3, NOD1, NLRP12, or NLRX1, were co-expressed with PKR in HEK293A cells. The physical interaction between PKR and these myc-tagged proteins is assessed by Co-immunoprecipitation (IP) and Western-blot (WB) analysis. Results are representative of two independent experiments.

Supplementary Fig. 29

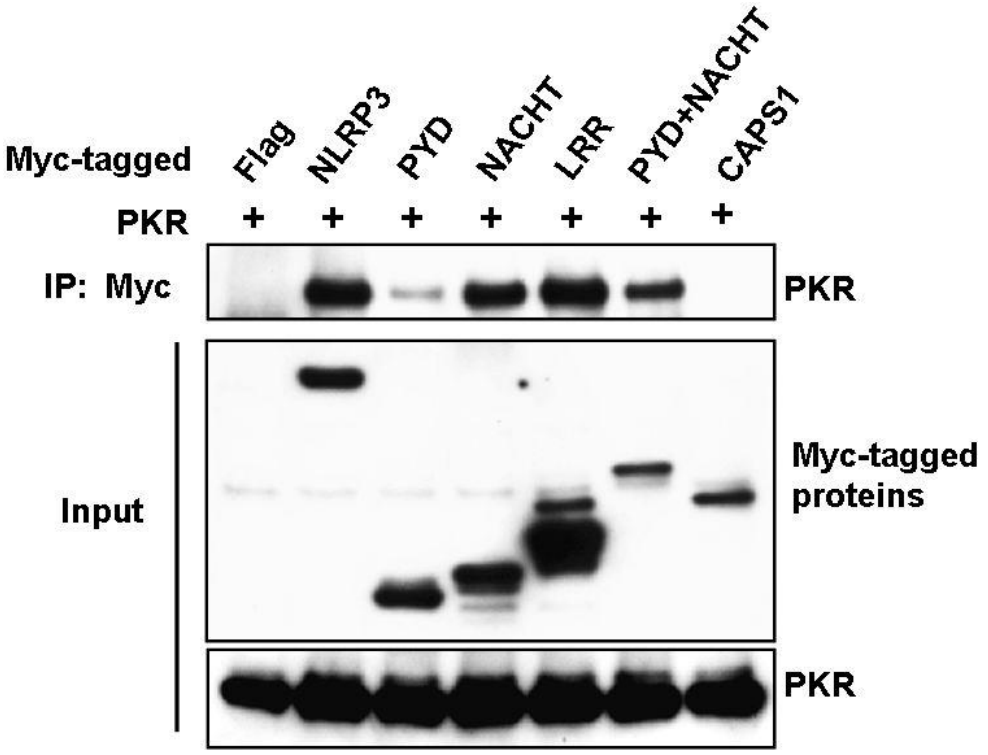

Supplementary Fig. 29. All three domains of NLRP3, including PYD, NACHT, and LRR, bind PKR. Myc-tagged Caspase-1, myc-tagged NLRP3, or myc-tagged truncated NLRP3 mutants (PYD, NACHT, LRR, and PYD+NACHT), were co-expressed with PKR in HEK293A cells. The physical interaction between PKR and these myc-tagged proteins is assessed by Co-immunoprecipitation (IP) and Western-blot (WB) analysis. Results are representative of two independent experiments.

Supplementary Fig. 30

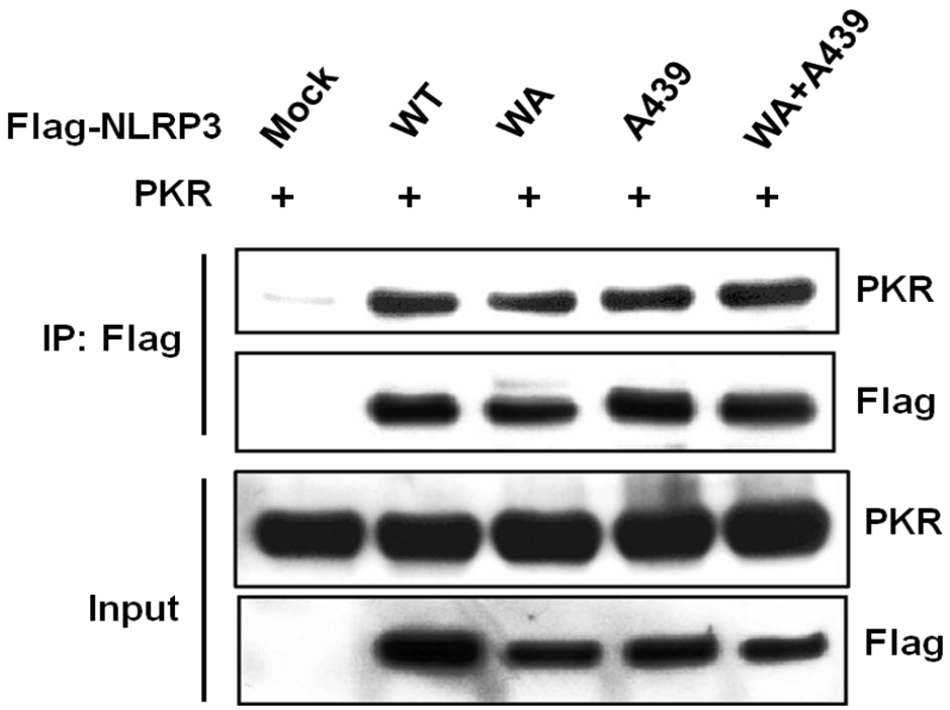

Supplementary Fig. 30. Both the "loss of function" (Walker A) NLRP3 mutant and the "enhance of function" (A439V) NLRP3 mutant bind PKR. Flag-tagged Wild-type (WT) NLRP3, Flag-tagged Walker A (WA) NLRP3 mutant, Flag-tagged A439V (A439) NLRP3 mutant, and Flag-tagged double (WA+A439) NLRP3 mutant, were co-expressed with PKR in HEK293A cells. The physical interaction between PKR and these Flag-tagged proteins is assessed by Co-immunoprecipitation (IP) and Western-blot (WB) analysis.

Supplementary Fig. 31

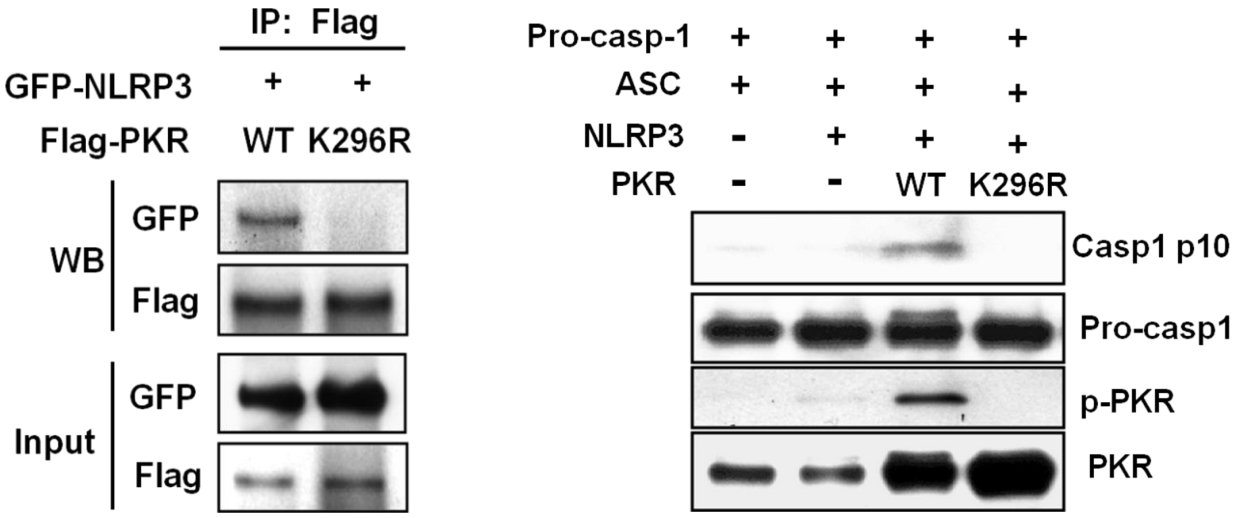

Supplementary Fig. 31. PKR K296R mutant does not bind NLRP3 and fails to activate the reconstituted NLRP3 inflammasome. HEK293A cells were transfected as indicated. The physical interaction of PKR mutants and NLRP3 was analyzed immunoprecipitation (IP) and Western-blot (WB) analysis (a). Caspase-1 activation was assessed by Western-blot (b). Results are representative of 2 independent experiments.

Supplementary Fig. 32

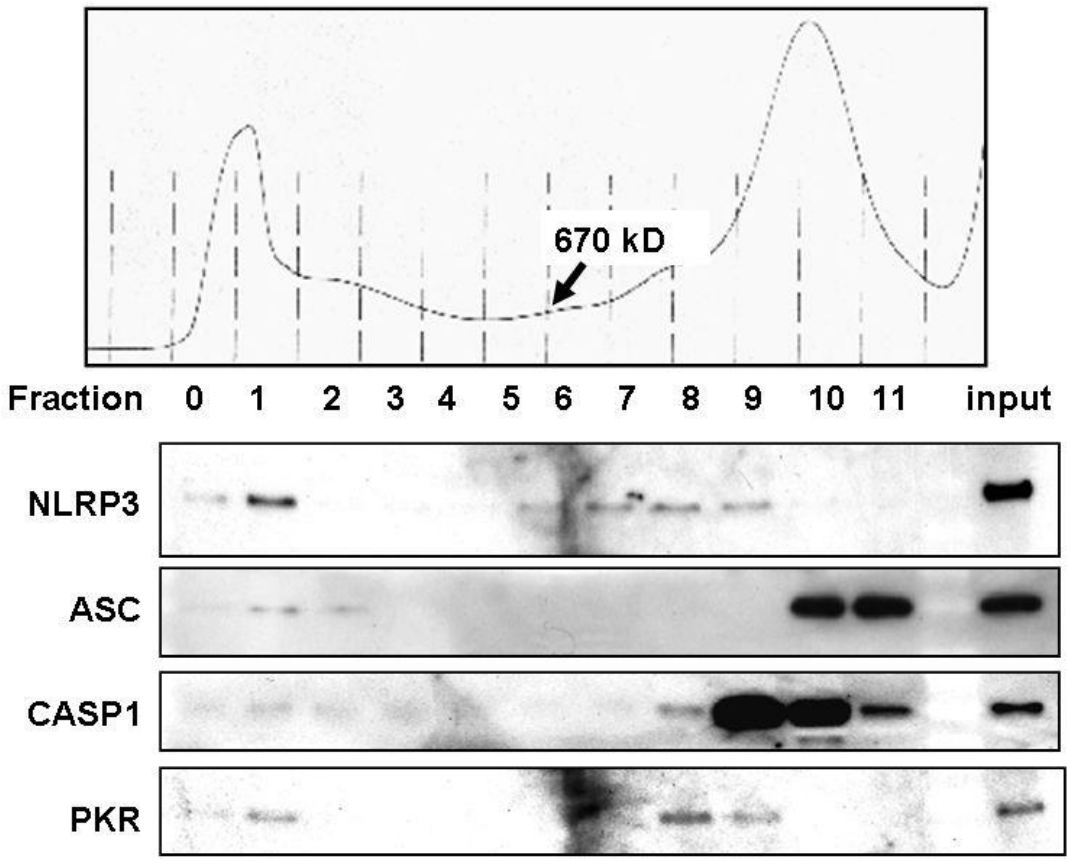

Supplementary Fig. 32. PKR and NLRP3 eluted together with ASC and caspase-1 in the same high molecular weight fraction of the ATP-stimulated macrophages extract. LPS-primed $PKR^{+/+}$ macrophages were stimulated with ATP. Fresh cell lysates were fractionated by gel-filtration. Levels of NLRP3, PKR, ASC, and Caspase-1 in each fraction were assessed by Western-blot. Results are representative of 2 independent experiments.

Supplementary Fig. 33

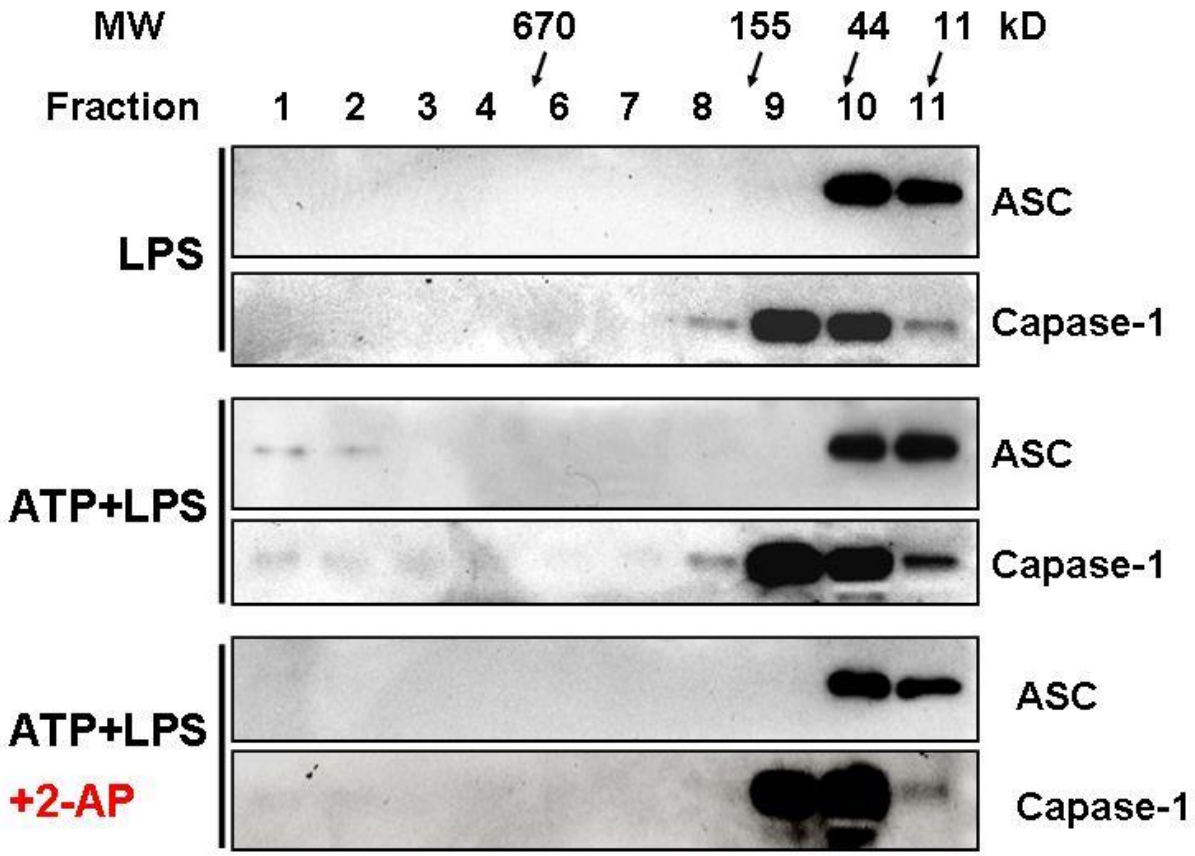

Supplementary Fig. 33. Pharmacological inhibition of PKR by 2-AP significantly reduced the level of ASC and Caspase-1 in the high molecular weight fraction containing NLRP3 and PKR. $PKR^{+/+}$ macrophages were stimulated and treated with 2-AP as indicated. Fresh cell lysates were fractionated by gel-filtration. Levels of NLRP3, PKR, ASC, and Caspase-1 in each fraction were assessed by Western-blot. Results are representative of 3 independent experiments.

Supplementary Fig. 34

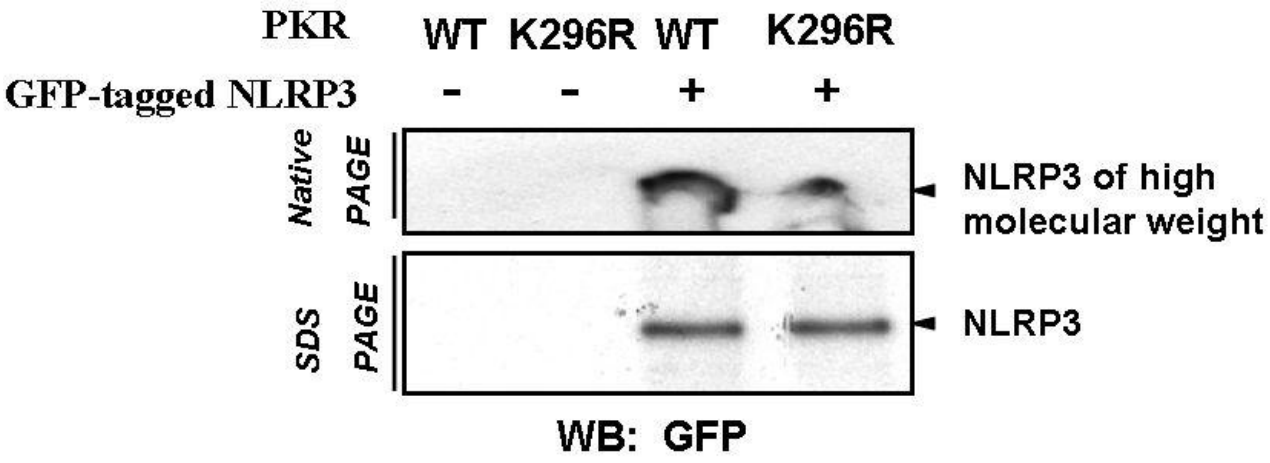

Supplementary Fig. 34. PKR facilitates the NLRP3 oligomerization. HEK293A cells were transfected as indicated for 24 h. Cell lysates were subjected to Native PAGE or SDS PAGE, followed by the measurement of the level of NLPR3 in high molecular weight fraction, and the total level of NLPR3 expression. Results are representative of 2 independent experiments.

Supplementary Fig. 35

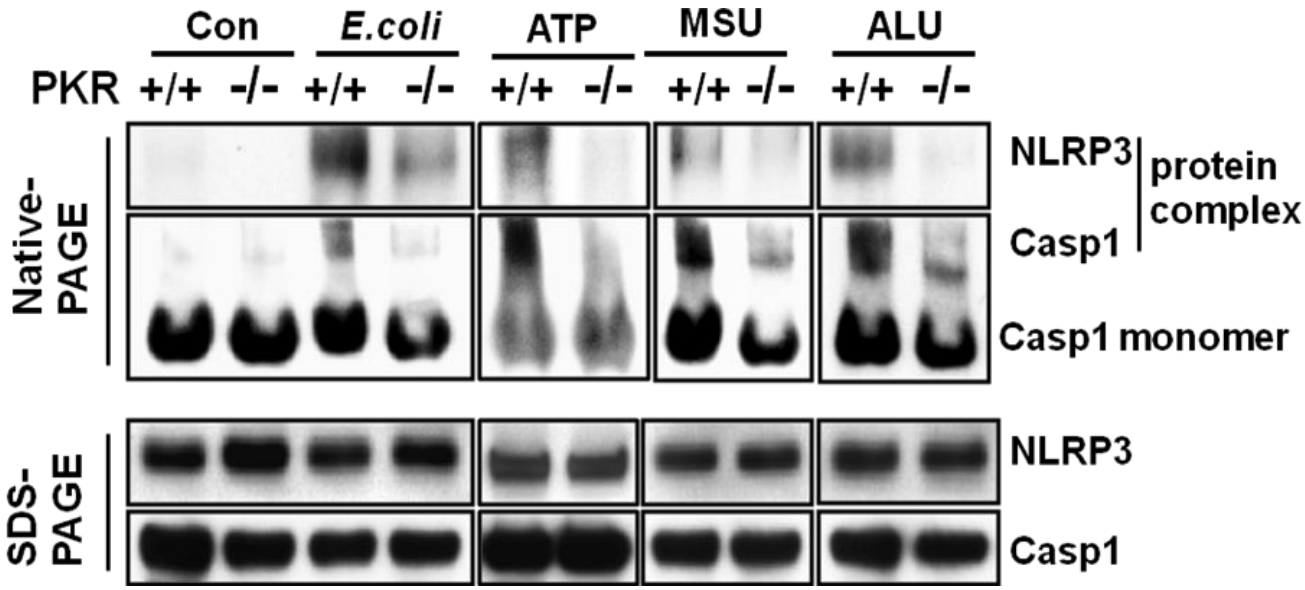

Supplementary Fig. 35. PKR deficiency impaired the NLRP3 inflammasome assambly. LPS-primed $PKR^{+/+}$ or $PKR^{-/-}$ macrophages were stimulated with ATP, MSU, ALU, or *E. coli*. Cell lysates were subjected to native-PAGE or SDS-PAGE, followed by the measurement of the level of NLPR3 and caspase-1 by Western blot. All results are representative of 2 independent experiments.

Supplementary Fig. 36

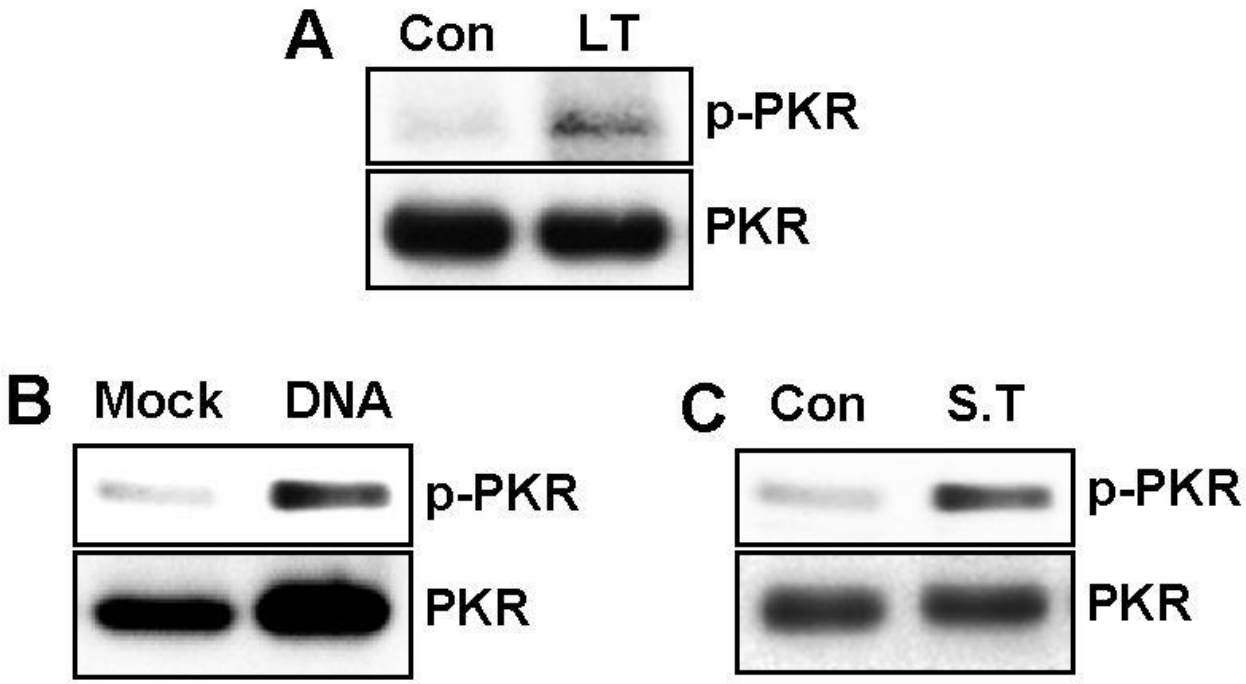

Supplementary Figure 36. Anthrax lethal toxin (LT), DNA transfection, or *S. typhimurium* exposure induces PKR phosphorylation. (A) LPS-primed $PKR^{+/+}$ macrophages were stimulated with LT for 1h. Cells were lysed 2h after stimulation and PKR activation was monitored by autophosphorylation. (B-C) PMA-differentiated THP-1 human macrophages were either transfected with Poly (dA:dT) by lipofectamine 2000 (B), or exposed to wild-type *S. typhimurium* (Multiplicity of Infection = 50) (C). PKR phosphorylation and total PKR level in cell lysates were assessed by western-blot. All results are representative of 3 independent experiments.

Supplementary Fig. 37

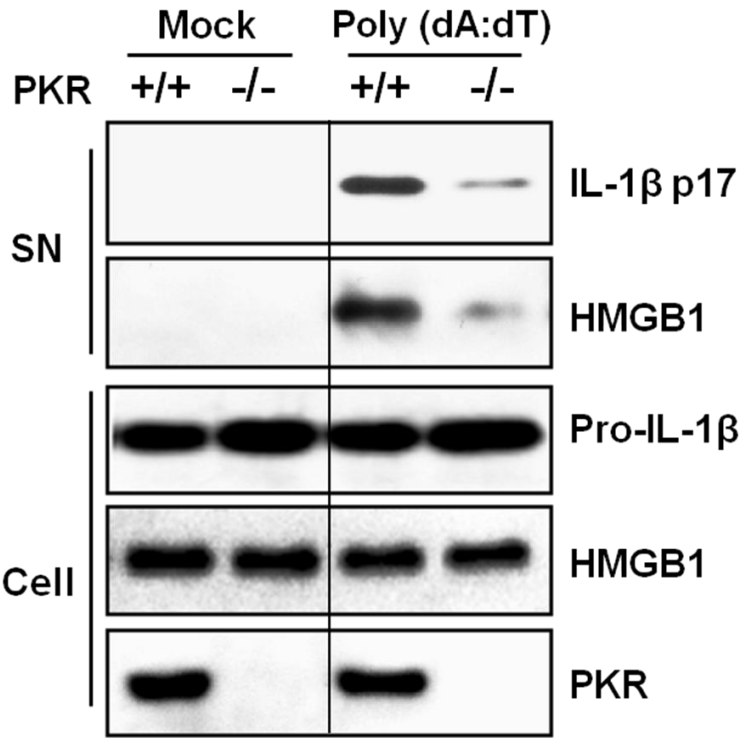

Supplementary Figure 37. PKR regulates DNA transfection-induced inflammasome activation. Ultra-pure LPS-primed macrophages from $PKR^{+/+}$ or $PKR^{-/-}$ mice were transfected with Poly (dA:dT)/Lyovec^{TM} for 6 h. Caspase-1 activation and IL-1β maturation was assessed by Western-blot. Results are representative of 3 independent experiments.

Supplementary Fig. 38

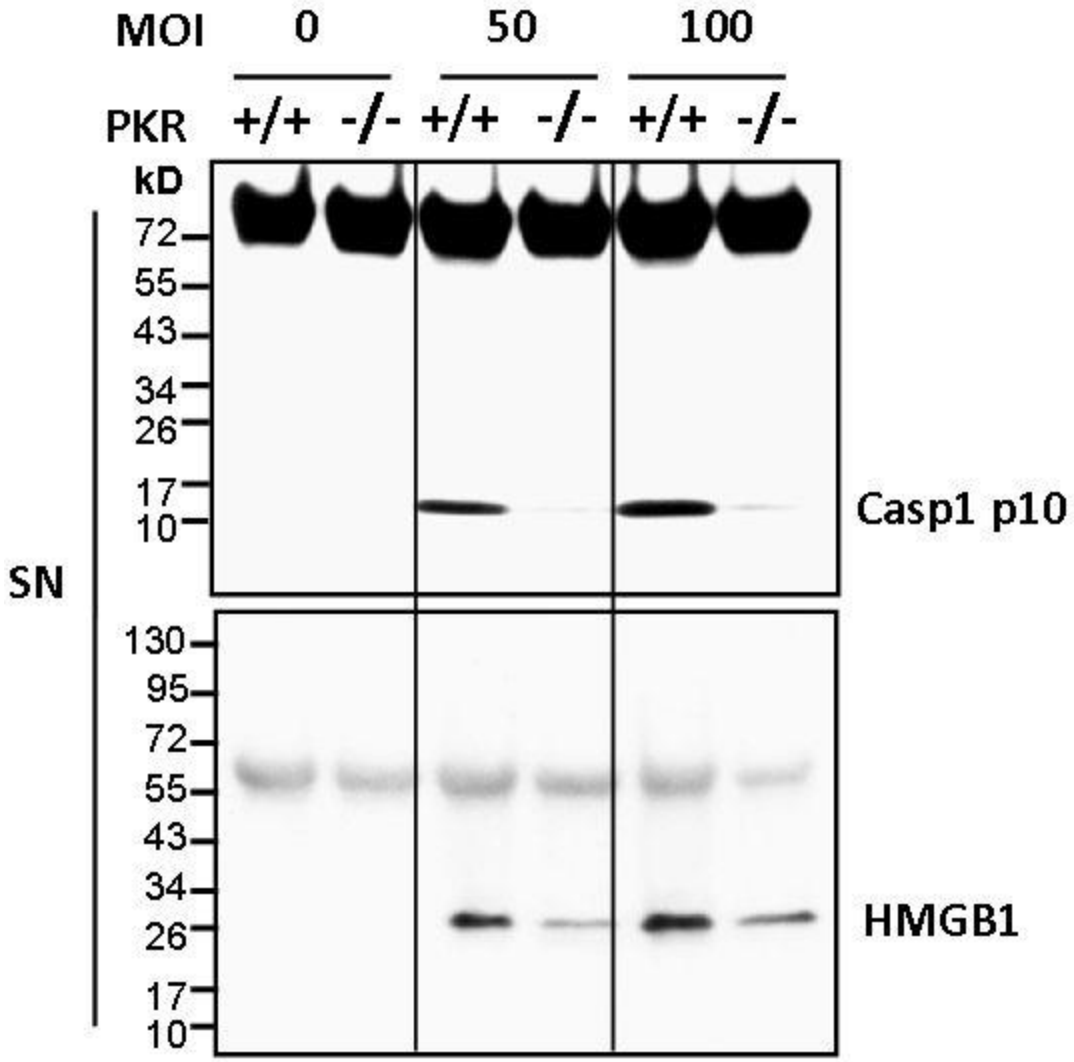

Supplementary Fig. 38. PKR regulates *S. typhimurium*-induced inflammasome activation. Unprimed $PKR^{+/+}$ or $PKR^{-/-}$ macrophages were infected with *S. typhimurium* (S.T) at the indicated multiplicity of infection (MOI) for 1h. Caspase-1 activation and HMGB1 secretion were assessed by Western-blot. All results are representative of at least three independent experiments.

Supplementary Fig. 39.

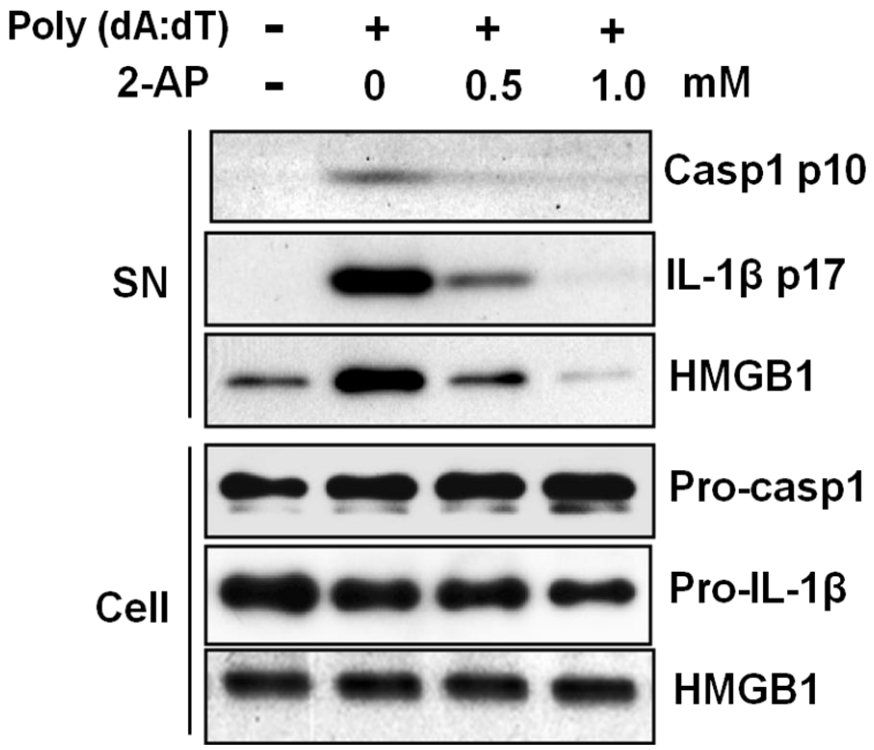

Supplementary Fig. 39. PKR inhibitor 2-AP dose-dependently inhibits Poly (dA:dT) transfection-induced inflammasome activation. Ultra-pure LPS-primed mouse macrophages from wild-type mice were transfected with Poly (dA:dT)/Lyovec^{TM} for 6 h in the absence or the presence of 2-AP at the indicated concentration. Caspase-1 activation, IL-1β maturation, and HMGB1 release were assessed by Western-blot. Results are representative of 3 independent experiments.

Supplementary Fig. 40

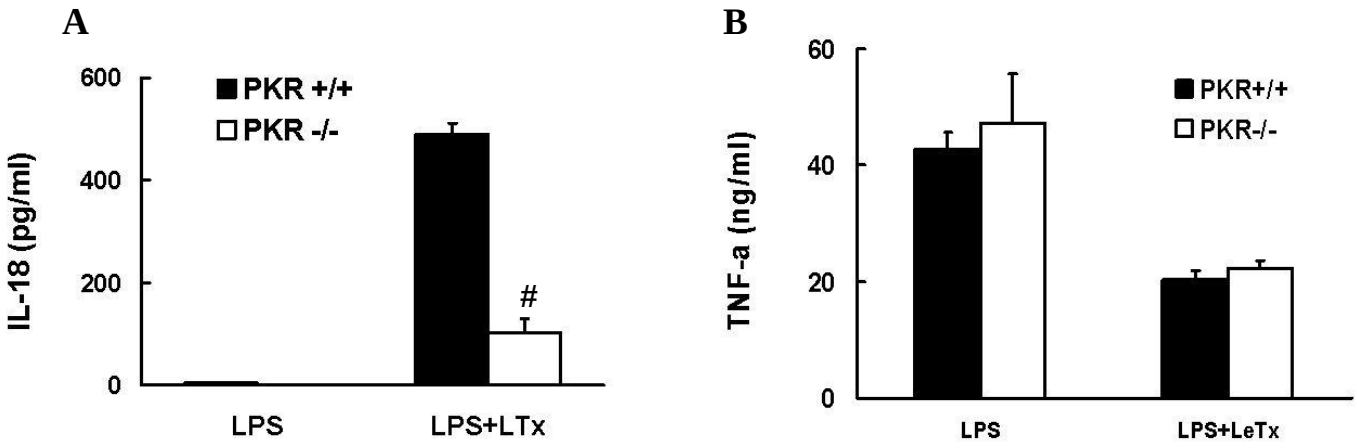

Supplementary Fig. 40. PKR regulates LT-induced IL18 release. LPS-primed $PKR^{+/+}$ and $PKR^{-/-}$ macrophages were stimulated with LT for 6h, IL-18 and TNF levels were measured in the supernatant by ELISA. Data shown are means ± SD. #, $p<0.05$ vs. wild-type stimulated groups.

Supplementary Fig. 41

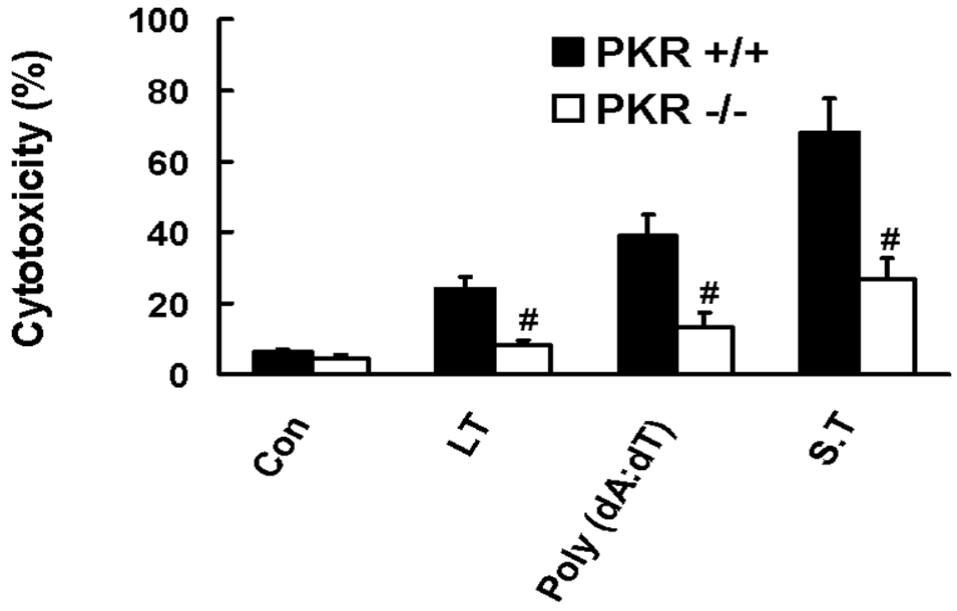

Supplementary Fig. 41. PKR regulates LT, Poly (dA:dT) transfection, or *S. typhimurium* infection-induced LDH release. LPS-primed $PKR^{+/+}$ and $PKR^{-/-}$ macrophages were exposed to LT, Poly (dA:dT) transfection, or *S. typhimurium* infection (MOI=50). Cytotoxicity was determined by LDH assay. Data shown are means ± SD. #, $p<0.05$ vs. wild-type stimulated groups.

Supplementary Fig. 42.

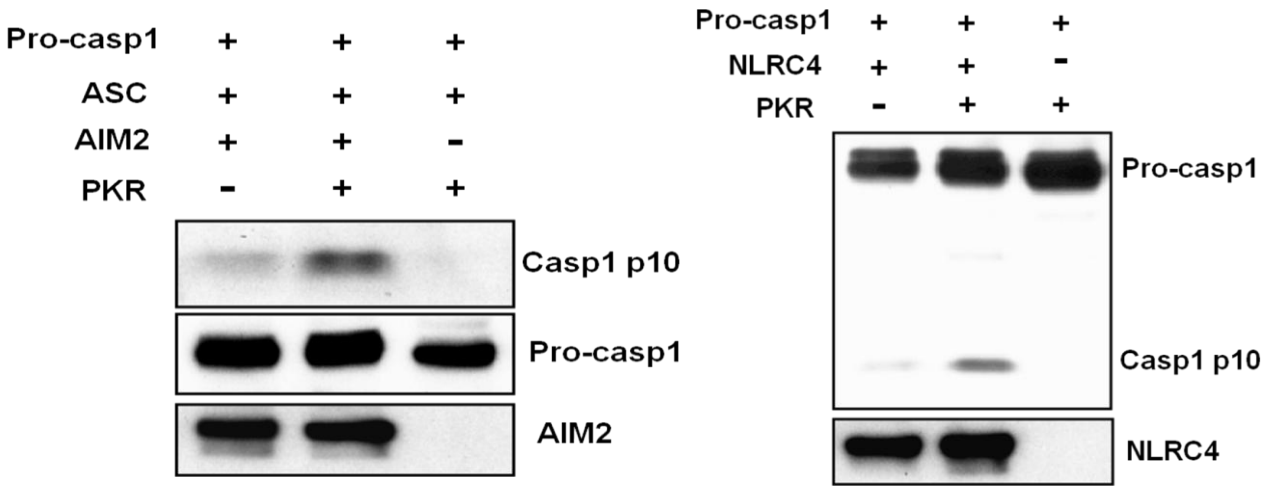

Supplementary Fig. 42. PKR overexpression significantly increased the activity of the reconstituted AIM2 or NLRC4 inflammasome. HEK293A cells were transfected as indicated. Caspase-1 activation was assessed by Western-blot. Results are representative of 2 independent experiments.

Supplementary Fig. 43.

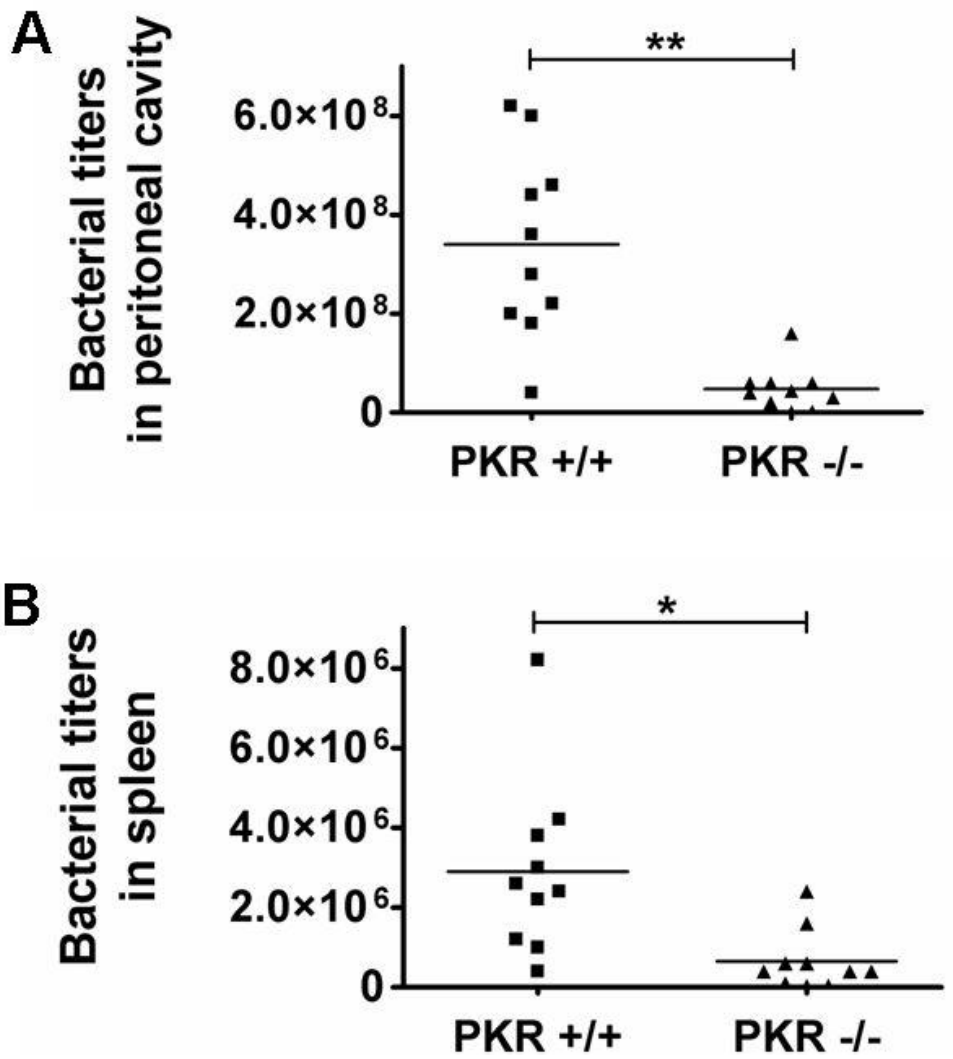

Supplementary Fig. 43. PKR$^{-/-}$ mice had significantly lower bacterial titers as compared to PKR$^{+/+}$ controls. PKR$^{+/+}$ or PKR$^{-/-}$ mice (n=10) were injected i.p. with live *E. coli* (2×10^9 per mouse). Bacterial titers in both peritoneal cavity and spleen were measured 24 hour after *E.coli* challenge. *****, $p<0.01$, ****** $p<0.001$; vs. wild-type controls.

Supplementary method: Mass Spec

To characterize the redox status of cysteine residues from extracellular HMGB1 derived from wild-type peritoneal macrophages, we employed liquid chromatography tandem mass spectrometric analysis (LC-MS/MS). Tryptic digestion and mass spectrometric characterization of HMGB1 derived from the culture media of cells stimulated with LPS produced peptides with the following molecular weights that contained C23 (1564.7 Da), C45 (618.3 Da) and C106 (2002.3 Da) (MS Figure 1A). Tandem mass spectrometric (MS/MS) analysis of b and y ions generated confirmed the amino acid sequence of each peptide and also the addition of an *N*-Ethylmalemide (NEM – mass shift 125 Da) adduct on C23 and C45 and an iodoacetamide adduct (mass shift 57 Da) localized to C106. These data reflect that C23 and C45 participated in a disulfide bond and that C106 was present in the thiol form (MS Figure 2A-F). In addition to these peptides, a molecule of 1993.3 Da was also identified in the cell culture media of cells treated with either ATP, MSU or ALU (MS Figure 1B). This peptide contained C106 and MS/MS analysis confirmed the terminal oxidation to a sulphonate derivative localized to C106. Importantly, peptides of predicted molecular weights of 550.5 Da and 1496.7 Da (C23 and C24 iodoacetamide adduct) and 2070.3 Da (C106 NEM adduct) were not detected. These data indicate that C106 did not participated in a disulphide bond or that neither C23 nor C45 were present in a reduced form. Following the induction of necrosis to peritoneal macrophages, cysteine containing peptides with the following molecule weights were detected for C23 (1496.7 and 1564.7 Da), C45 (550.5 and 618.3 Da) and for C106 (2002.3 Da) (MS Figure 1C). MS/MS analysis confirmed only an iodoacetamide adduct on C106 (MS Figure 2A) and both iodoacetamide and NEM adducts on both C23 and C45 (MS Figure

2C-F). No terminal oxidation was observed on any cysteine residue derived from HMGB1 present in the culture media following the induction of necrosis. As seen previously these data confirm that both C23 and C45 formed a duisluphide bond (C23-S-S-C45) or were present in a reduced form. C106 was only present as a thiol (C106-SH).

Characterization of HMGB1 acetylation status following cellular stimulation of the induction of necrosis

The acetylation status of both HMGB1 nuclear localization sequences were characterized and quantified by mass spectrometry as previously described [1] following Glu-C digestion of HMGB1 derived from peritoneal macrophages. Stimulation of cells with one of LPS, ATP, MSU or ALU resulted in the production of HMGB1 derived peptides with the molecular weights of 1749.8 and 1342.6 Da following MS analysis representing NLS 1 and 2 respectively (MS Figure 1D). A second round of MS/MS confirmed the acetylation of each lysine residue within each peptide (MS Figure 2G). In contrast, the Glu-C digestion of HMGB1 derived from the culture media of necrotic cells did not yield 1749.8 and 1342.6 Da peptides (MS Figure 1E). However, peptides with the molecular weights of 1623.8 and 1132.6 Da were detected. MS/MS analysis of b and y ions generated following a second round of MS/MS confirmed the amino acid sequence of each peptide to represent both NLS 1 and 2 respectively. The mass shift of 126 Da for NLS 1 and 210 Da for NLS 2 represents the loss of either 3x acetyl or 5x acetyl modifications from either NLS 1 or 2 respectively. These data indicate that HMGB1 present in the culture media of LPS, ATP, MSU or ALU stimulated cells

was only acetylated with the NLSs and that derived from necrosis was only present in a non-acetylated form at each NLS.

All chemicals and solvents were purchased from Sigma, if not otherwise stated, and were of the highest grade available. Briefly, supernatants were pre-cleared with 50ul protein G-Sepharose beads for one hour at 4°C. Pre-cleared supernatant HMGB1 were immunoprecipitated with 5ug anti-HMGB1 antibody (Abcam ab18256) for 16hours at 4°C. The redox dependent modifications of each cysteine residue was characterized by mass spectrometry as previously described with some minor modifications [2]. Free thiol groups within HMGB1 were first alkylated with 10mM iodoacetamide at 4°C for 90min. Cysteine residues present in disulfide bonds were reduced with 30mM dithiothreitol (DTT) at 4°C for one hour followed by alkylation of newly formed thiol groups with 90mM *N*-Ethylmaleimide (NEM) at 4°C for 10min. Samples was then subjected to trypsin (Promega) digestion according to manufacturer's instructions. ZipTip C18 (Millipore) tips were used to desalt peptide digests prior to liquid chromatography electrospray tandem mass spectrometry (LC-MS/MS). The characterization and absolute quantification of acetylated HMGB1 was determined as previously described following Glu-C (New England Biolabs) digestion of HMGB1 [1].

(1) Antoine, D.J. *et al.* J. Hepatol. **56,** 1070-1079 (2012).

(2) Yang, H. *et al.* Mol Med. **18,** 250-259 (2012).